Review in Advance first posted online on September 11, 2013. (Changes may still occur before final publication online and in print.)

Wake Signature Detection

Geoffrey R. Spedding

Department of Aerospace and Mechanical Engineering, University of Southern California, Los Angeles, California 90089; email: geoff@usc.edu

Annu. Rev. Fluid Mech. 2014. 46:273–302

The *Annual Review of Fluid Mechanics* is online at fluid.annualreviews.org

This article's doi:
10.1146/annurev-fluid-011212-140747

Keywords

stratified turbulence, islands, turtles, seals, copepods

Abstract

An accumulated body of quantitative evidence shows that bluff-body wakes in stably stratified environments have an unusual degree of coherence and organization, so characteristic geometries such as arrays of alternating-signed vortices have very long lifetimes, as measured in units of buoyancy timescales, or in the downstream distance scaled by a body length. The combination of pattern geometry and persistence renders the detection of these wakes possible in principle. It now appears that identifiable signatures can be found from many disparate sources: Islands, fish, and plankton all have been noted to generate features that can be detected by climate modelers, hopeful navigators in open oceans, or hungry predators. The various types of wakes are reviewed with notes on why their signatures are important and to whom. A general theory of wake pattern formation is lacking and would have to span many orders of magnitude in Reynolds number.

1. INTRODUCTION

Most life on Earth, and likely on all inhabitable planets, is one immersed in fluids. To the sensory systems of such life forms, the fluids are close to transparent, and if the motion of solid bodies in the fluids is evident, the fluid motions themselves are not. Absent detailed and global information, the fluid environment appears as a complex, and often turbulent, sea of fluid motions at many scales. However, as our detection systems on Earth improve—most particularly those that show information from a near-Earth orbit—the apparent frequency of patterns, and perhaps underlying order in these motions, has increased. The air and sea are not information-free but contain traces from many influences, both current and past ones. This review investigates how certain patterns can be long-lived and traced back to the generating conditions. The original applications are related to naval operations, but the overall scope is much broader, ranging from the effect of large island wakes, with scales of hundreds of kilometers, on climate models to the detection of hydrodynamic trails by small animals of millimeter scale.

To maintain focus, plumes are not considered in detail, for which reviews by Settles (2006) and Woods (2010) may be consulted. The surface wakes of ships, treated in Reed & Milgram (2002), are also not considered. Aircraft contrails are another category that deserve their own review and are omitted for reasons of space alone. Lin & Pao (1979) surveyed early experiments in stratified turbulence, and Riley & Lelong (2000) reviewed mathematical, computational, and experimental work for flows with strong stratification. These will be our starting point.

The title of the review may be something of a misnomer because the focus is on hydrodynamic conditions that create wakes that can, in principle, be detected, spending very little time on how detection works in each case. In every instance, the detection aspect has much to be discovered.

2. STRATIFIED WAKES: A CANONICAL CASE

2.1. Dimensionless Numbers

In oceans and atmosphere, flows at various scales are commonly described in terms of the dimensionless parameters

$$\mathrm{Re} = \frac{UL}{\nu}, \quad \mathrm{Fr} = \frac{U}{NL}, \quad \text{and} \quad \mathrm{Ro} = \frac{U}{fL}, \tag{1}$$

which describe the balance between forces from fluid motions at characteristic speeds U, and length scales L, with kinematic viscosity ν, background stratification N, and rotation f. In the ocean, stratification ultimately comes from the differential heating of the sea surface by the sun, together with variation with depth of salinity, and the atmospheric density gradient comes from the hydrostatic variation of pressure and density with height above Earth's surface. It is reasonable to model the variation of density with height, z, as a linear function for the lower 10 km of the atmosphere and the top 40–500 m of the open ocean, when the Brunt-Väisälä frequency, $N = -[(g/\rho_o)/(\partial\rho/\partial z)]^{1/2}$, in units of radians per second is a natural internal oscillation frequency of fluid particles of equilibrium density ρ_o with uniform gravitational acceleration, g. Thus the internal Froude number, Fr, is a ratio of two timescales: a convective timescale L/U and an internal wave period $1/N$. Similarly, the Rossby number, Ro, expresses the relative importance of timescales $1/f$, where $f = 2\Omega \sin\phi$ is the Coriolis frequency at latitude ϕ, and Ω is the planetary rotation rate.

We may identify a class of flows called mesoscale flows in which the length and timescales are not so large as to be affected by planetary-scale motions and not so small as to be immediately suppressed by either buoyancy or viscous forces. Reynolds numbers are high enough to allow the full spectrum of turbulent motions, yet when energy inputs are intermittent in space or time, the

decaying kinetic energy of the flow is eventually strongly influenced by buoyancy (and then by viscosity). Let us consider a wind speed of 10 m/s over an island 10 km in length. In air, we find that Re $\approx 7 \times 10^9$, and for $N = 10^{-2}$ rad/s, $f = 10^{-4}$ per second at midlatitudes, Fr ≈ 0.1, and Ro ≈ 10. Under the water surface, around a thermocline, if $U = 1$ m/s and $N = 10^{-3}$ rad/s, then one obtains Fr ≈ 0.1 and Ro ≈ 1. Over island-type scales, buoyancy is immediately dominant, in both air and water, while rotation will eventually become significant as length and timescales increase in the far wake. Anticipating a major motivation for part of this work, let us also consider an underwater vehicle with diameter $D = 10$ m, and $U = 10$ m/s; then in the same thermocline, we find Re $\approx 10^8$, Fr $\approx 10^3$, and Ro $\approx 10^4$. Neither stratification nor rotation will be significant in early wakes of such objects, but because characteristic local flow speeds decrease and length scales increase as the wake decays far from the body, the local Fr, and eventually Ro, will be $\mathcal{O}(1)$ or lower.

Below we see that not only are certain components of the velocity field very persistent, and slowly changing in time, but they also show a striking degree or order and pattern. The pattern geometry comes partly from the initial conditions, so, arguing backward, the wake can contain information on its creator. This has potential consequences for those who would wish to find wake makers, from satellite-borne observation platforms to biological predator-prey relations. The stability and longevity of pattern formations also have implications for appropriate modeling in global circulation models.

2.2. Basic Phenomenology

It is convenient to study the development of initially turbulent bluff-body wakes in stably stratified fluids by towing spheres horizontally through a linear density gradient, created by continuously varying the concentration of dissolved salt in a stationary tow tank. Adjusting the tow speed, the body diameter, and strength of the density gradient, and hence N, allows systematic variation of Re and Fr. Examples of these experimental studies are provided by Afanasyev (2004), Bonneton et al. (1993), Chomaz et al. (1993), Lin et al. (1992), Meunier & Spedding (2006), Spedding (1997), and Spedding et al. (1996a,b). The approximate ranges of Re and Fr are [100–10^4] and [0.1–100], respectively.

The characteristic geometry of the towed sphere wake in a stratified fluid can be seen in **Figure 1** (see the sidebar PIV Measurements in Stratified Flows). The initial Reynolds number, Re $\approx 5 \times 10^3$, and Froude number, Fr ≥ 10, are sufficiently high so that close to the sphere, the flow is turbulent and apparently disorganized. Yet by the time the first reliable observations can be made, some degree of order can be seen. The instantaneous vertical vorticity field is not just a patch of random fluctuations: The negative- and positive-signed vorticity regions occupy expected positions based on an imagined time-averaged velocity profile, and the patches of vorticity themselves are not completely irregular. The apparent degree of order, or smoothness, of the coherent structures increases with time, as small-scale fluctuations dissipate, while larger vortices remain. Once formed, the vortex structures interact through merging of like-signed neighbors. Other than a variation in length scale due to different size spheres, the pattern of $\omega_z(x, y)$ in the right column at $Nt = 240$ does not depend in an obvious way on the initial value of Fr.

While the ω_z field is slowly evolving, the divergence field, Δ_z, can be used as an indicator of internal waves, and **Figure 2** shows $\omega_z(x, y)$ and $\Delta_z(x, y)$ at three times during a regime we call a nonequilibrium regime, as the initially energetic and dominant turbulence decays and is gradually constrained by the stable background density gradient. **Figure 2** shows periodic wave packets being emitted from the wake. In the later time step ($Nt = 79$), the most-clear wave packets are traceable to the largest vortex structures in $\omega_z(x, y)$. If the vortex structures have a regular pattern,

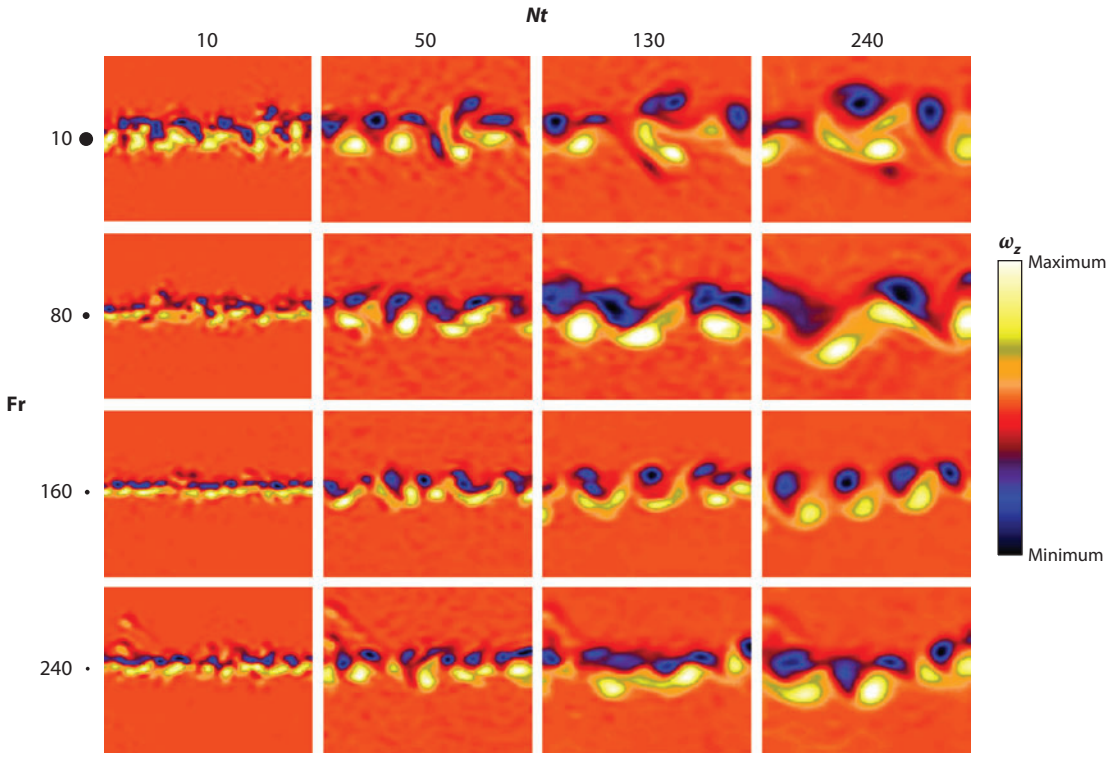

Figure 1

The time evolution of initially turbulent stratified wakes. A sphere with a diameter proportional to the left column of circle silhouettes has passed the observation window from right to left. The Reynolds number, Re, is from 5 to 10×10^3, and the Froude number, Fr, is given in the left column. Time is from left to right and is given in units of Nt on top. The vertical vorticity, $\omega_z(x, y)$, is mapped onto the color bar on the right, locally scaled each time step between $\pm|\omega_z|_{\max}$. Figure replotted from original data in Spedding (1997).

PIV MEASUREMENTS IN STRATIFIED FLOWS

Particle imaging velocimetry (PIV) methods in stratified fluids have certain conveniences and certain challenges. A significant convenience is that tracer particles can be sorted by density so that they all rest in equilibrium on a single density surface (isopycnal). At moderate to late times ($Nt \geq 10$), the projection of the motions onto a horizontal plane $\{x, y\}$ gives estimates of the two horizontal velocity components, $\mathbf{q} = \{\mathbf{u}, \mathbf{v}\}$, and one may then readily calculate gradient quantities,

$$\omega_z = \nabla \times \mathbf{q} \text{ and } \Delta_\mathbf{z} = \nabla \cdot \mathbf{q},$$

which are the approximate experimental analogs of the decompositions into vortical and wave modes of Riley et al. (1981) and Lilly (1983). At earlier times, or in making cuts through different planes, such as $\{x, z\}$, for example, special care needs to be taken to avoid artificial measurement turbulence from refractive-index gradients caused by perturbation in the density field. Refractive-index matching techniques have been reviewed by Amini & Hassan (2012).

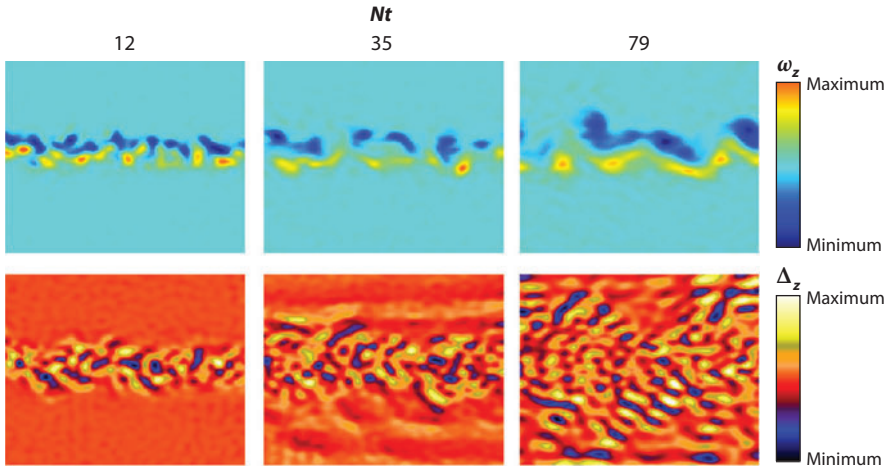

Figure 2

Vortex and wave motions in a nonequilibrium wake. Three time steps are shown (in *Nt*, across the top) of vortex (ω_z) and wave (Δ_z) modes in a wake with Re = 5,800 and Fr = 20.

then internal wave packets originating there can retain this information. A recurring theme will be that regular arrays of coherent structures in wake flows are associated with the longevity and persistence of the pattern. The term coherent structure is used as a convenient descriptive term, without rigorous justification, upon which a large literature rests. For a thoughtful discussion of the notion of coherent structures, readers are referred to Holmes et al. (2012, chapter 2).

The surprising degree of order in the slowly varying $\omega_z(x, y)$ component of the stratified wake has certain quantitative consequences. One can make the usual equivalence between observations that vary over time in a stationary laboratory frame of reference and an effective wake length in x as $Ut = x$. Then in parameters that involve stratification or buoyancy, we can write

$$\frac{x}{D} = \frac{\mathrm{Fr}}{2} Nt. \tag{2}$$

Streamwise-averaged profiles of the u component of velocity, $U_X(y)$, are self-similar and well approximated with a Gaussian, whose amplitude and width give measures of velocity and length scales in the developing far wake. **Figure 3** presents a summary of late-wake measurements, and four points can be made. (*a*) The wake width, L_y, grows as $(x/D)^{1/3}$. Horizontal growth rates might be expected to increase, compared with an unstratified wake because, at some point, expansion in the vertical direction will be suppressed by the stratification. However, this is not the case. The horizontal growth rates are the same as for an unstratified fluid. This result is independent of Fr. (*b*) Vertical growth rates, $L_z(x/D)$, are reduced, and the initial wake height is almost constant. Subsequent growth is approximately as $(x/D)^{1/2}$. (*c*) During the time when horizontal growth rates are the same as those for the unstratified wake, but the vertical growth is almost zero, one may infer that a wake-averaged kinetic energy density will decrease more slowly. Accordingly, the mean centerline defect velocity decays more slowly than its unstratified counterpart until the vertical wake growth phase begins. At this point, the mean centerline flow speed, U_0, is approximately 10 times what it would have been in the absence of stratification. (*d*) A Strouhal number can be defined as

$$\mathrm{St} = D/\lambda_x, \tag{3}$$

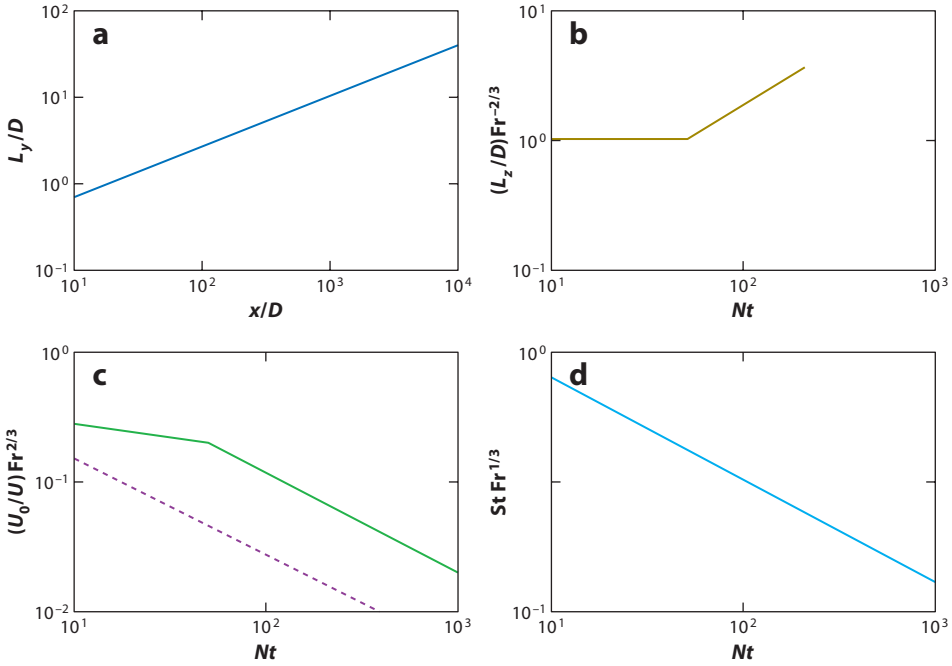

Figure 3

Sketches of self-similar evolution in stratified wakes, for Re > 4,000, Fr ∈ {4,240}. (*a*) $L_y \sim (x/D)^{1/3}$, indistinguishable in this respect from a nonstratified wake. (*b*) L_z initially grows negligibly until $Nt \approx 80$, at which point it evolves as $Nt^{1/2}$. (*c*) The initial decay of the mean wake defect is as $Nt^{-1/4}$, so when it begins to decay at the same rate as a nonstratified wake (*dashed purple line*) (again at $Nt \approx 80$), the magnitude is always higher. The slow decay rate at intermediate times is characteristic of all stratified wakes and marks a nonequilibrium regime, where the flow adjusts to the ambient, stable density field. (*d*) St evolves as $Nt^{-1/3}$. Similar to L_y in panel *a*, it shows no variation through the end of the nonequilibrium regime at $Nt = 80$. Panels *b–d* are given as functions of Nt, but the power-law behavior in x/D is the same.

where λ_x is the streamwise spacing between successive like-signed vortices $\lambda_x \sim L_y$, so St $\sim (x/D)^{-1/3}$.

2.3. The Claim of Universality

The wake properties summarized in **Figure 3** were observed at all Re and Fr tested. It was particularly surprising to see that variations in Fr were unimportant, but the reason is because all wakes, no matter how energetic and turbulent their initial starting point, will eventually become dominated by the background stratification, and now the local, effective Fr is very small. The initial conditions, set by Fr, are not important. One may enquire to what extent other types of initial and boundary conditions are also forgotten in the late wake evolution.

2.3.1. The effect of the body/initial conditions. Meunier & Spedding (2004) repeated the basic sphere experiment with a hemisphere, a disk, a cube, and a 6:1 aspect ratio cylinder and prolate spheroid. Sharp-edge bodies had comparatively wider and more energetic wakes, whereas streamlined bodies had narrower and less energetic ones. Arguing along the classical lines of Tennekes & Lumley (1972) and Townsend (1976), one may define a length scale that depends on

the drag of the body,

$$F_D = \rho \frac{\pi D_{\text{eff}}^2}{4} U_B^2, \tag{4}$$

where the entrained fluid has an effective diameter D_{eff} within which it has acquired the same speed as the body, U_B. For axisymmetric bodies, there is now a simple relation between the drag coefficient, C_D, and this new length scale,

$$D_{\text{eff}} = D\sqrt{\frac{C_D}{2}}. \tag{5}$$

As a first estimate, C_D can be found from references in the literature for unstratified flows, a strategy that should work reasonably well for high-Fr wakes. D_{eff} can be used to define an effective Froude number,

$$\text{Fr}_{\text{eff}} = \frac{2U_B}{N\ D_{\text{eff}}}. \tag{6}$$

When the mean centerline velocity U_o, the horizontal wake width L_y, and the Strouhal number St were appropriately normalized as $(U_o/U_B)\text{Fr}_{\text{eff}}^{2/3}$, L_y/D_{eff}, and $\text{St}_{\text{eff}} = D_{\text{eff}}/\lambda_X$, the downstream evolution of each quantity collapsed onto one curve (just as in **Figure 3**), showing no other sign of the different initial conditions.

There is some evidence that true self-similar collapse of both mean and turbulence quantities in turbulent wakes in unstratified fluids may not occur until very long distances, if at all (see Bevilaqua & Lykoudis 1978, Johansson et al. 2003). However, within experimental uncertainty, Meunier & Spedding (2004) showed that self-similar fluctuating velocity profiles could be measured in the bluff-body wakes and that a turbulent Reynolds number, based on the assumption of a constant turbulent eddy viscosity, could be calculated, having an approximate value of 15 ± 5 in the far wake. The relative amplitude of the fluctuating velocity magnitudes initially varied with body shape (angled, nonstreamlined bodies had higher initial u_o'), but in the late wake, these differences vanished.

It was concluded that there was no memory in the late wake of the initial conditions, other than some rescaling that depends on the body drag. Therefore, given an appropriate momentum thickness length, D_{eff}, in all measurable respects, late wakes in stratified flows evolve similarly, regardless of body shape.

2.3.2. Numerical simulations. Almost all numerical simulations concerning turbulent, stratified wakes are initialized with no body at all, but start with some prescribed mean and turbulence profiles. The simulation must begin with a profile shape for both mean and turbulence quantities and their relative amplitudes, and then initial values are taken from quantities in the literature, usually from experimental data in unstratified fluids. The first simulations of the initially turbulent wake in a stratified fluid by Gourlay et al. (2001) (direct numerical simulation), Dommermuth et al. (2002) (large-eddy simulation), and Diamessis et al. (2005) (large-eddy simulation) differed somewhat in the details of the initial conditions, but all produced late wake flows with coherent vortices whose geometry and time evolution of the mean length and velocity scales agreed quite well with experiment. It was notable that the coherent structures emerged with no deliberate seeding, so their formation was shown to be a general characteristic of the initially turbulent wake and not a remnant of some more specific upstream geometry.

2.3.3. Higher Reynolds numbers. One of the attractions of the numerical simulations is the potential access to much higher Reynolds numbers than are easily available in a physical laboratory, and recent simulations (e.g., Diamessis et al. 2011) have shown similar scaling laws up to $\text{Re} = 10^5$,

about an order of magnitude higher than most experiments. In the interim, detailed experiments by Bonnier et al. (1998, 2000) and Bonnier & Eiff (2002) had shown that the structure and dynamics of the late-wake vortices are independent of Fr and initial conditions and that these vortex structures are similar in density and velocity perturbation for both laminar and turbulent wakes. By exploiting symmetries in initial conditions or simply through improved computing power, investigators have performed increasingly fine-resolution simulations at higher Reynolds numbers, for systems of vortices, box-filling turbulence, and wakes with and without net momentum. As Re increases, there is an increase in the vertical shear between the quasi-horizontal, large-scale vortices and Kelvin-Helmholtz instabilities then can continuously generate small-scale turbulence, which could, in principle, destabilize or disrupt the larger-scale vortices. This has been discussed by Riley & de Bruyn Kops (2003), Waite & Bartello (2003), Brethouwer et al. (2007), Deloncle et al. (2008), Augier & Billant (2011), Diamessis et al. (2011), and Augier et al. (2012a). It seems that the large-scale separation between the secondary instabilities and the coherent structures whose decorrelation and vertical shearing cause them assures that the large structures are not significantly disrupted, even at large Re. Observations of large-scale structures in island wakes that persist for many hundreds of kilometers also provide proof of the possible existence and longevity of coherent structures at high Re.

Voropayev & Afanasyev (1994) pointed out that the scale separation between synoptic or planetary motions and those involving dissipation at small scales is very large, and that moderate- to low-Re dynamics may correctly represent large-scale ocean dynamics because the small-scale turbulence that rides along the large-scale motions acts like a turbulent eddy viscosity, having a value many (seven to eight) orders of magnitude higher than the molecular value. The idea is known in the geophysical research literature, and Barton (2009) gave an empirical relation between a length scale of interest, L, and an effective horizontal eddy viscosity, K_L, of

$$K_L(\mathrm{m}^2/\mathrm{s}) = 2.2 \times 10^{-4} L^{1.13} \tag{7}$$

and noted that typical ocean values of K_L range from 10^2 to 10^5 m^2/s. Many presumably very-high-Re structures seen in satellite imagery do resemble low-Re viscous flows, and laboratory modeling of such flows has not always systematically exploited the similarity. Of course, the existence and dynamical scale separation in high-Re flows cannot be presumed a priori, but if the patterns are stable, then the empirical convenience is quite appreciable.

2.3.4. Momentumless wakes. A self-propelled body makes a wake with zero net momentum because thrust and drag balance and could evolve differently, as had been reported for both unstratified (Higuchi & Kubota 1990, Schetz & Jakubowski 1975) and stratified (Lin & Pao 1974, 1979; Schooley & Stewart 1962) fluids. Meunier & Spedding (2006) conducted experiments with a self-propelled, streamlined body that was also towed. The balance between the propeller thrust and body drag could thus be varied independently, and the ratio was held constant throughout any given traverse of the tank, assuring steady, unaccelerated motion.

The results were surprising in many respects. First, at the momentumless condition, there was no similar shape to a profile of the streamwise-averaged velocity in the wake. The usual conception of the wake as a superposition of two sets of mean profiles, with the net sum having two axisymmetric lobes representing thrust and drag components, was not applicable. The profile of velocity fluctuations, $u^* = <u'^2 + v'^2>^{1/2}$, was also not regular in shape, so true similarity scaling cannot be sought. A maximum of the fluctuation profile could be measured and decayed with downstream distance. $u^*_{\max}$ was always significantly smaller than that for the equivalent towed body, but its decay rate (approximate power-law behavior was seen) was lower, contrary to most expectations and the observations of Lin & Pao (1979). No consistent Froude number scaling

collapsed the experimental data, and different curves were observed for different sized propellers on the same body. Similar conclusions were obtained from measures constructed from the more robust streamwise-averaged vorticity profiles. No consistent scaling could collapse stratified wake data from exactly self-propelled bodies.

The second surprising finding was that all other wakes, either overthrusted or underthrusted, could be successfully rescaled onto the same curves as previously reported for drag wakes. Once again, the scaling depended only on the net momentum flux, and for all cases in which the body speed was just 2% or more away (either over or under) from the exact self-propelled speed, the evolution of mean and turbulence quantities was well described by single power-law exponents.

It can be further argued that practical instances of exact zero net momentum are vanishingly rare. A self-propelled body in a stable stratification will generate internal waves, whose contribution to the total drag will not remain in the wake region, and the wake itself will be away from the momentumless condition. Variations in the ambient by more than $\pm 2\%$ will be the norm, and any nonsteady motion will also move the wake away from this precise self-propelled point. Therefore, in practice, although exact self-propelled wakes are not universal or general, all other wakes, including those likely to be found in nature or ocean applications, are.

2.3.5. General laws for stratified wakes. A general length scale, for any wake, propelled or not, can be calculated as a momentum thickness,

$$D_{\text{mom}} = D\sqrt{C_D/2}\sqrt{|1-(U_C^2/U_B^2)|}, \tag{8}$$

which depends on the drag coefficient, as before, and also on the ratio of the body speed, U_B, to the critical speed, U_C, at which the wake will be exactly momentumless. From experiment, we have the following universal relationships for all stratified wakes. Characteristic wake widths scale as

$$\frac{L_y}{D_{\text{mom}}}\text{Fr}_{\text{mom}}^{-0.35} = 0.275\,(Nt)^{0.35}; \tag{9}$$

mean wake defect velocities are

$$\frac{|U_o|}{U_B}\text{Fr}_{\text{mom}}^{0.76} = 6.6\,(Nt)^{-0.76}; \tag{10}$$

and the Strouhal number is

$$\text{St}_{\text{mom}}\text{Fr}_{\text{mom}}^{0.34} = 0.823\,(Nt)^{-0.34}, \tag{11}$$

where the momentum Froude number is defined as

$$\text{Fr}_{\text{mom}} = \frac{2U_B}{ND_{\text{mom}}}. \tag{12}$$

For towed bodies, D_{mom} and Fr_{mom} can be replaced directly by D_{eff} and Fr_{eff}, respectively, as in Equations 5 and 6.

2.4. Practical Consequences

Interestingly, Equations 9–11 have Froude number scalings that, through Equation 2, can be seen to be independent of the Froude number or stratification. Moreover, the general scaling exponents for the wake width and velocity magnitude are not distinguishable from their nonstratified counterparts. However, as seen in **Figures 1** and **2**, the pattern of the wake is also very coherent. It is the persistence of a coherent pattern that makes detection possible. **Figure 4** shows that a putative submerged detector of either energy or enstrophy could easily find the late wake, up

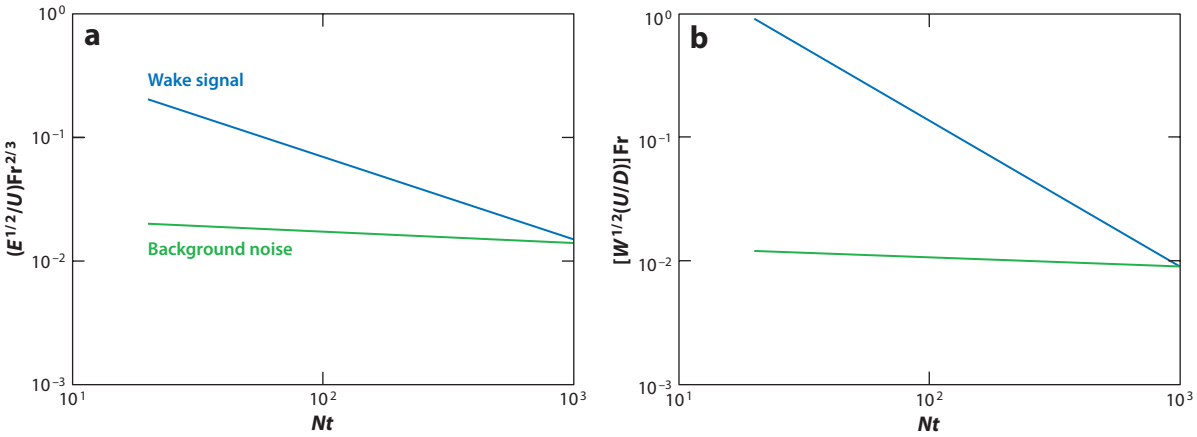

Figure 4

The wake signal (*blue*) exceeds the background noise (*green*) for long times. Both the (*a*) wake-averaged energy (*E*) and (*b*) enstrophy (*W*) are easily detectable, even in the absence of pattern/geometric information, for times that scale out to ≥10 days in an ideal (quiet) ocean. Figure redrawn from Spedding et al. (1996b).

to $Nt \approx 10^3$. If $N \approx 10^{-3}$, then $t \approx 10^6$ s, so detection is possible, in principle, for 280 h or approximately 12 days.

The rather extraordinary slow time variation, or persistence, is not unexpected. The governing equations for strongly stratified motions in a Boussinesq fluid have been given by Riley & Lelong (2000):

$$\frac{\partial \mathbf{u}_b}{\partial t} + \mathbf{u}_b \cdot \nabla_b \mathbf{u}_b = -\nabla_b p + \frac{1}{\alpha^2}\frac{1}{\mathrm{Re}_L}\nabla^2 \mathbf{u}_b, \tag{13a}$$

$$\nabla_b \cdot \mathbf{u}_b = 0, \tag{13b}$$

$$0 = -\frac{\partial p}{\partial z} - \rho, \tag{13c}$$

$$\frac{\partial \rho}{\partial t} + \mathbf{u}_b \cdot \nabla_b \rho - w = \frac{1}{\alpha^2}\frac{1}{\mathrm{ScRe}_L}\nabla^2 \rho, \tag{13d}$$

where the b subscripts refer to the horizontal components, Sc is a Schmidt number, and Re_L is a turbulent Reynolds number. Here $\alpha = L_V/L_H$ is a ratio of vertical and horizontal length scales, set in some way by the initial conditions preceding the small-Fr limit. As the authors noted, these equations have some interesting properties, one being that Equations 13a and 13b are two-dimensional, nonlinear equations, and describe a particular kind of quasi-two-dimensional motion, as originally described by Riley et al. (1981) and Lilly (1983). Nothing in Equations 13a and 13b prescribes any variation in the vertical direction, which is given in Equations 13c and 13d, in which vertical pressure gradients are balanced by density variations (Equation 13c), and then a diffusion equation links w with variations in ρ. Lilly (1983) argued that at high Re, adjacent horizontal layers would decouple in the vertical direction and that strong shearing motions between them could then generate small-scale overturning instabilities. This prediction has been partially borne out in recent numerical simulations, in particular those of Riley & de Bruyn Kops (2003) and Diamessis et al. (2011), as previously noted. It was also pointed out that in the absence of rotation,

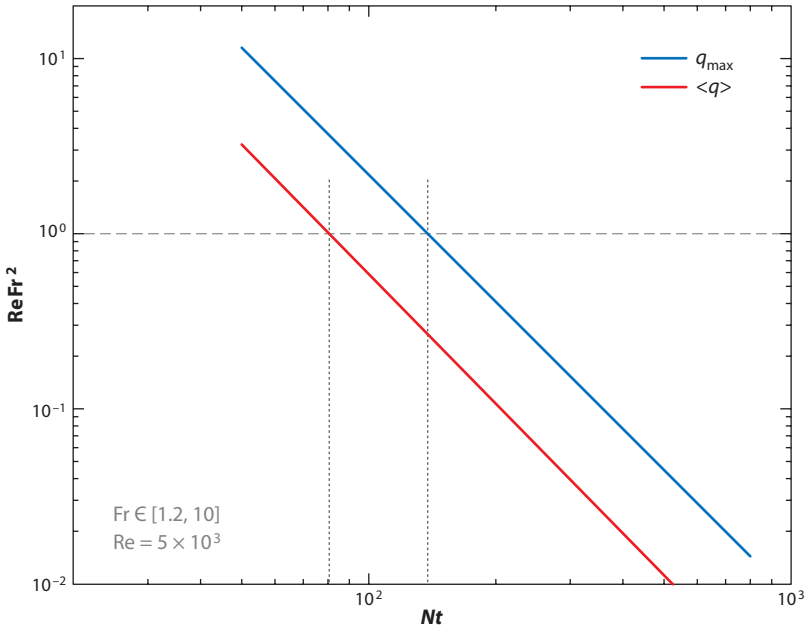

Figure 5

Decaying, stratified wake turbulence evolution in laboratory experiments. A criterion of $\mathrm{ReFr}^2 \geq 1$ can be used to determine when a strongly stratified flow is not simply dominated by viscous decay. In a typical experiment, measures of both the local Reynolds number and local Froude number based on turbulent length and velocity scales decay, but the $\mathrm{Re}\cdot\mathrm{Fr}^2$ product can remain >1 for $Nt \geq 80$, with the margin depending on whether wake-averaged or maximum values are used.

the evolution of the vertical vorticity could be written as

$$\frac{\partial}{\partial t}\omega_z + \mathbf{u}_b \cdot \nabla \omega_z = \frac{1}{\alpha^2}\frac{1}{\mathrm{Re}_L}\nabla^2 \omega_z. \tag{14}$$

In the absence of viscous diffusion, the vertical component of vorticity is conserved following a fluid element. This observation is quite consistent with the persistent late wakes in laboratory experiments. Equations 13c and 13d allow nonzero vertical velocities (unlike a truly two-dimensional flow), so internal wave solutions are also possible.

The selection of the vertical length scale remains to be settled in this analysis, and Billant & Chomaz (2001) argued that stratified flows will self-select a length scale, $L_V \sim u'/N$, when a buoyancy Reynolds number $R = \mathrm{ReFr}^2 \gg 1$. In most laboratory experiments, even if they are initially small, viscous terms become dominant quite quickly and $R \leq 1$ (**Figure 5**); experiments by Godoy-Diana et al. (2004) that controlled the initial vertical scale independently show there is no scale selection by the viscous-controlled flow, whose vertical structure diffuses at viscous timescales and possibly preserves other, initial vertical length scales. The existence of two strongly stratified regimes, with $R > 1$ and $R < 1$, controlled by different scaling parameters, has since been noted in analysis and numerical experiments by a number of authors, including Augier & Billant (2011), Brethouwer et al. (2007), Lindborg (2006), and Augier et al. (2012b).

In summary, the experimental evidence for strong pattern generation comes from a strongly stratified but ultimately viscosity-influenced regime that has dynamics that differ from the much

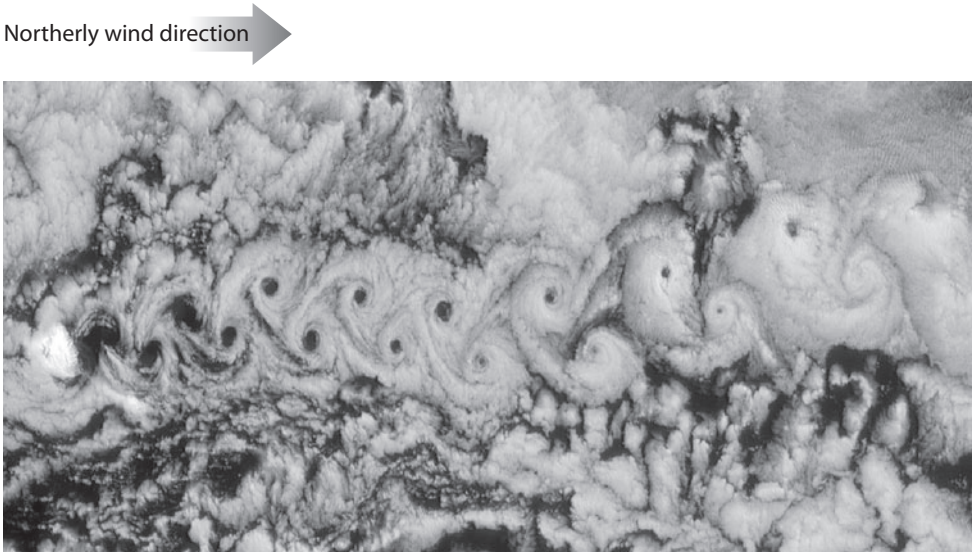

Figure 6

Vortex street behind Jan Mayen Island in an image taken from the NASA *Terra* satellite, using one downward-looking camera on the Multiangle Imaging Spectroradiometer (MISR). Northerly winds run from left to right, and the streamwise observation length is 365 km. Image courtesy of NASA/GSFC/LaRC/JPL and the MISR team.

higher Re flows found in many practical applications, either naval or geophysical. Nevertheless, current evidence suggests that large-scale patterns, once formed, do not destabilize in the presence of secondary instabilities that are quite remote in wave-number space. Empirical observations also suggest that coherent patterns are preserved far downstream of islands and other prominent topographies (see the next section).

3. ATMOSPHERES AND OCEANS

Our earthbound view of the mostly transparent seas and atmosphere has been substantially enlarged through space-based observation platforms. When clouds, sediment suspensions, algal blooms, sea ice, or surface wave patterns permit, striking and beautiful images emerge of a fluid environment that is rich in structure and patterns. This section provides a small number of examples, with interpretations that refer back to the general examples above. Two specific examples, with relevance to climate modeling and to sea turtle navigation, are examined in slightly more detail to show how the phenomenon of persistent wakes can be important.

3.1. Pattern and Coherence

Figure 6 shows the wake behind the Beerenberg volcano on Jan Mayen Island, located approximately 650 km northeast of Iceland. The volcano height is 2.2 km above sea level. The vortex wake pattern is readily observable for at least 350 km. If we take a characteristic scale at half height of approximately 1 km, then $(x/D)_{\max} = 350$. Supposing wind speeds of $U = 10$ m/s, then we find that Re $\approx 10^9$ and Fr ≈ 1, if there is a stratified layer around the island. One might argue that the absence of wave-like disturbances on the wake implies that the stratification, if present, is weak. In either case, the wake persistence is not unexpected, given the isolated location and strong

possibility of persistent winds. The spacing of island wake vortices has been measured by Young & Zawislak (2006), who compiled measures of an aspect ratio, $A = \lambda_x/\lambda_y$, and width, $W = \lambda_y/D$. For a sample of 30 wake images from the *Aqua* and *Terra* satellites, $A = 0.37 \pm 0.02$ and $W = 1.8 \pm 1$. In a classical Kármán vortex street, $A = 0.28$. The higher measured spacing was attributed to the turbulent, diffusive growth of the wake vortices. Indeed, St defined previously in Equation 2 can be written $\mathrm{St} = 1/(AW)$, and its value from island wakes is 1.5. The value is much higher than seen in laboratory data, which typically varies from 0.5 to 0.1 over the wake lifetime, but the laboratory data are always in the far-wake region. Increased wake spacing in far wakes can be expected.

The literature on the remote sensing and modeling of atmospheric and ocean phenomena is large and growing, as examples accumulate and as concerns mount on changing global climate patterns. Recent overviews and updates can be found in Robinson (2004, 2010) and Barale et al. (2010). Specific examples of sensing and modeling island wakes may be found in Barton (2009), Barton et al. (2001), Dong & McWilliams (2007), Dong et al. (2007), Pao & Kao (1976), and Wolanski et al. (1984).

High-frequency radar data can yield high-resolution ocean surface velocity fields that can resolve mesoscales and now allow new flow structure analysis and detection procedures, most notably in Lagrangian coherent structure (LCS) identification and tracking (see Haller 2001, 2002). LCS are most commonly identified through forward and/or backward calculation of finite-time Lyapunov exponents (FTLEs) that characterize the expansion rate of initially neighboring fluid parcels and have been shown to be quite practical in identifying coherent structures and transport properties (Shadden et al. 2005). Examples specific to geophysical flows include tracking through general circulation models (Beron-Vera et al. 2010), high-resolution local ocean circulation models (Veneziani et al. 2005), combined satellite altimetry and drifter data (Beron-Vera et al. 2008), surface current observations in Monterey Bay (Shadden et al. 2009), and pollution trails off the coast of Florida (Lekien et al. 2005).

3.2. Consequences for Climate Modeling

A spectacular example of a persistent island wake with significant dynamical and modeling consequences was described by Xie et al. (2001). The Hawaiian Islands are located far from any major landmass and are immersed in steady northeasterly trade winds. The islands themselves vary in size and maximum height: Maui has a 3-km peak, and the big island of Hawaii rises to 4.2 km. In the summertime, a temperature inversion layer is common at a height between 1 and 2 km. The islands have significant wind wakes that merge to form a persistent wake defect that is observable in the wind vorticity and divergence maps for 3,000 km to the west. It is thought that the wind wakes then cause Rossby waves in the ocean and that these are responsible for the appearance of a persistent warm-water band on a current from the west toward the islands. This band is known as the Hawaiian Lee Countercurrent, and **Figure 7** shows it to extend even further to approximately 8,000 km west of the Hawaiian Island chain.

The Hawaiian Islands' influence is over a spectacularly large range, although $x/D \approx 1{,}600$ is well within the bounds we have encountered thus far for wake longevity. Over such long planetary length and timescales, simple extrapolation of laboratory experiments in nonrotating flows is much too simplistic, but we do have another example of topography-generated disturbances that have far-reaching effects. Because the forcing is initially at the mesoscale, it would be easy for a modest grid resolution general circulation model to entirely miss the phenomenon. Further investigation of the response of a high-resolution, three-dimensional, regional atmospheric model (Hafner & Xie 2003) and of the individual island-induced topographic effects (Sasaki et al. 2010; Yang et al.

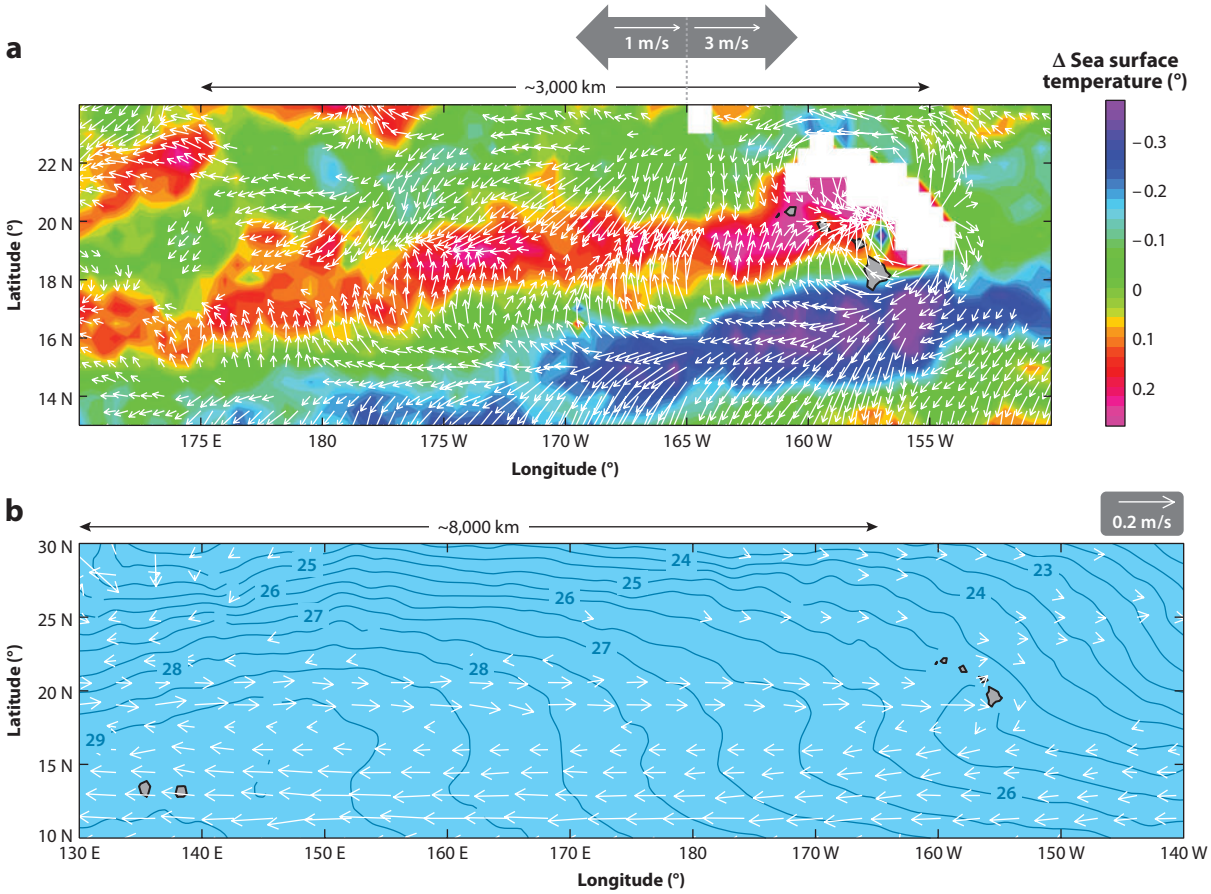

Figure 7

Extended wake-induced disturbances from the Hawaiian Islands. (*a*) The colors show the fluctuating sea-surface temperatures in degrees Celsius, and the wind vectors are scaled to the reference of 1 m/s to the left of 165W and to 3 m/s to the right. The distance from the Hawaiian Island chain at 155W to 175E is approximately 3,000 km. (*b*) The effect of the original wind forcing is felt for even longer distances in subsurface currents. Current vectors come from a high-resolution general circulation model, shown for a depth of 37.5 m, averaged from 1992 to 1998. Superimposed are contours in degrees Celsius of observed sea-surface temperatures from the *TRMM* (*Tropical Rain Measuring Mission*) satellite, averaged over 1999 (*dark blue lines*). The agreement between model-derived data and observations is good, and the horizontal scale from 155W to 130E is approximately 8,000 km. Figure redrawn from Xie et al. (2001) with permission from AAAS.

2008a,b) supports the notion that wind wake forcing of a long-length-scale geophysical process, such as Rossby waves, can then generate a significant feature in the subsurface currents. The large influence of the island wakes is important in signature detection from the point of view of the climate modeler, and it is a clear example of a (comparatively) small source having a large and persistent impact.

3.3. Consequences for Sea Turtles and Other Navigators

The generality of empirical findings from laboratory experiments in stratified wakes encourages extrapolation to more general cases, and it is possible that certain features of the pattern generation

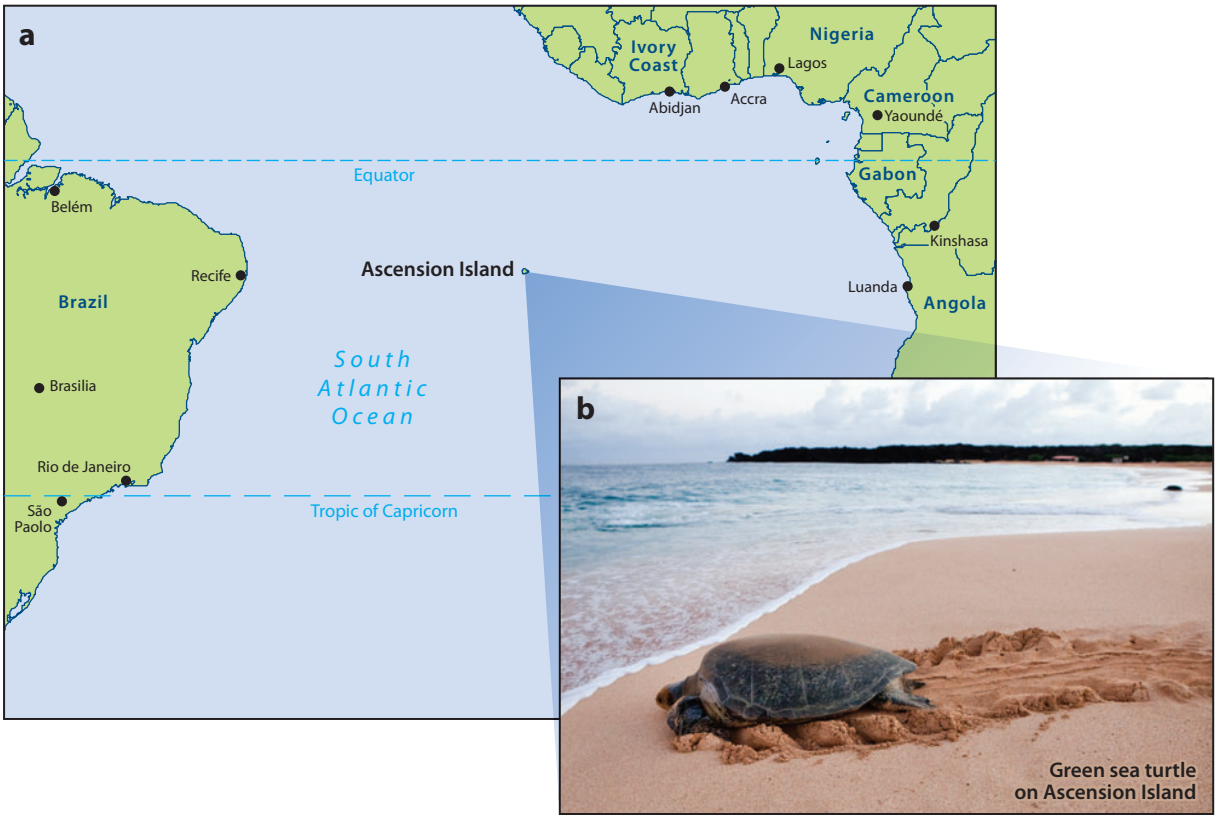

Figure 8

Sea turtle navigation. (*a*) Ascension Island, where Brazilian green turtles lay their eggs, is far from the nearest landmass. (*b*) A green sea turtle on Long Beach, Ascension Island, returns to the sea after egg laying. Panel *b* taken from National Geographic Stock, photographer Kent Kobersteen (picture ID 1397892).

and wake persistence at mesoscales in oceans and atmospheres have similar dynamics. In cases in which topographies are exposed to steady forcing, then the generation of information-rich trails may be expected and could be used in the ecosystem that has grown up around it.

3.3.1. The life cycle of the sea turtle. The large impact of a small source may be relevant in a quite different context. Here we explore the possibility that conditions leading to the longevity and preservation of information in ocean and atmospheric wakes could help explain some stubborn mysteries in animal navigation.

The Brazilian green turtle presents a case of seemingly improbable navigational ability over large distances with nonobvious information access (one of several noted in Alerstam et al. 2003). The newly hatched sea turtle emerges onto a sandy beach on Ascension Island, an isolated volcanic outcrop in the southern Atlantic Ocean, located approximately 1,600 km west of the coast of southern Africa and 2,200 km from the east coast of Brazil (**Figure 8**). It swims out into the surf and then to feeding grounds off the Brazilian coast. After 2–3 years, the females return to Ascension Island to lay eggs, which they do in a number of clutches over 11–13 days, swimming out to sea between each episode. The turtles then make their way back to Brazil, a journey that takes approximately 40 days.

The original return journey to Ascension Island requires an almost uncanny homing sense. The island is roughly circular, with a volcanic peak of 800 m and base diameter of around 10 km. At a distance of 2,200 km, a straight shot would require a pointing accuracy of less than one-third a degree. This kind of dead-reckoning system would be quite impractical in the face of varying and unpredictable changes in water currents, and it has long been recognized that systems for both orientation and navigation must be present. There are two types of navigation proposed for possible use by the migrating turtle. The first is a bicoordinate geomagnetic map in which any location can be determined by the combination of information from the magnetic field strength and inclination. The second type of navigation system would use information released by the island itself. These could be visual clues, wave pattern modification, and possible wakes or chemical plumes released in the air, water, or both. Some ingenious catch-release-track experiments have been conducted to test various possibilities.

3.3.2. Tracking experiments. **Figure 9*a*** shows seven complete or partial tracks of green turtles who were captured at the end of the egg-laying season and outfitted with a satellite transmitter and six powerful magnets whose field orientation varied with the animals' movement, thus masking all possible use of magnetic navigation clues. The paths of the magnetically disabled turtles did not vary from a control group who had only brass bars in the same attachment geometry. Navigation is clearly possible without magnetic clues. When female adult turtles are caught on the Ascension Island beaches at the beginning of the egg-laying season, a different set of experiments is possible, and Luschi et al. (2001) described the results of experiments after animals were transported by ship to locations northeast, southeast, west, and northwest of the island, displaced 60–450 km from their original positions. At the beginning of the egg-laying season, the turtles may be assumed to have a strong incentive to return to their beach, and 10 of the 18 did so. The displaced turtles would start off in apparently random directions and would then follow circuitous loops before settling on a trajectory that took them directly to the island. The average distance of this lock-on was approximately 100 km. **Figure 9*b*** shows that many would return along a northwest track. There was no evidence of the turtles following geomagnetic gradients from other locations around the island, and the behavior and success rate were consistent with the notion that some kind of signal from the island was followed.

The complete picture is less simple. Green turtles do have a magnetic sense that can discriminate both latitude and longitude (Putnam et al. 2011), and the use of magnetic information in positioning and orientation has been demonstrated by Lohmann et al. (2004). For a succinct summary, readers are referred to Lohmann (2010).

It is more than likely that a number of systems can be switched in and out according to navigational needs and the sensory data available, but the available evidence does raise questions. If the green turtle has a geomagnetic sense, then why was this apparently not used in the displacement experiments? Why was the westward navigation possible, even when all magnetic senses were disrupted? What other kinds of information are available from the natural environment? The following section is somewhat speculative in nature but attempts to put the navigation problem in a slightly different context, as suggested by the preceding sections on bluff-body and island wakes.

3.3.3. How to find a dot in the ocean. The eastward navigation of the female green sea turtle offers a paradigmatic case of surprising navigational accuracy, in which a very small tolerance for error can be supported. Advances in satellite telemetry seem only to raise the awareness of the difficulties involved. The feats include the following: (*a*) the ability to locate a very small, apparently isolated target destination by following a straight course; (*b*) the ability to continue to travel at night, even with no visible moon (in fact, because turtles are myopic out of the water, many kinds

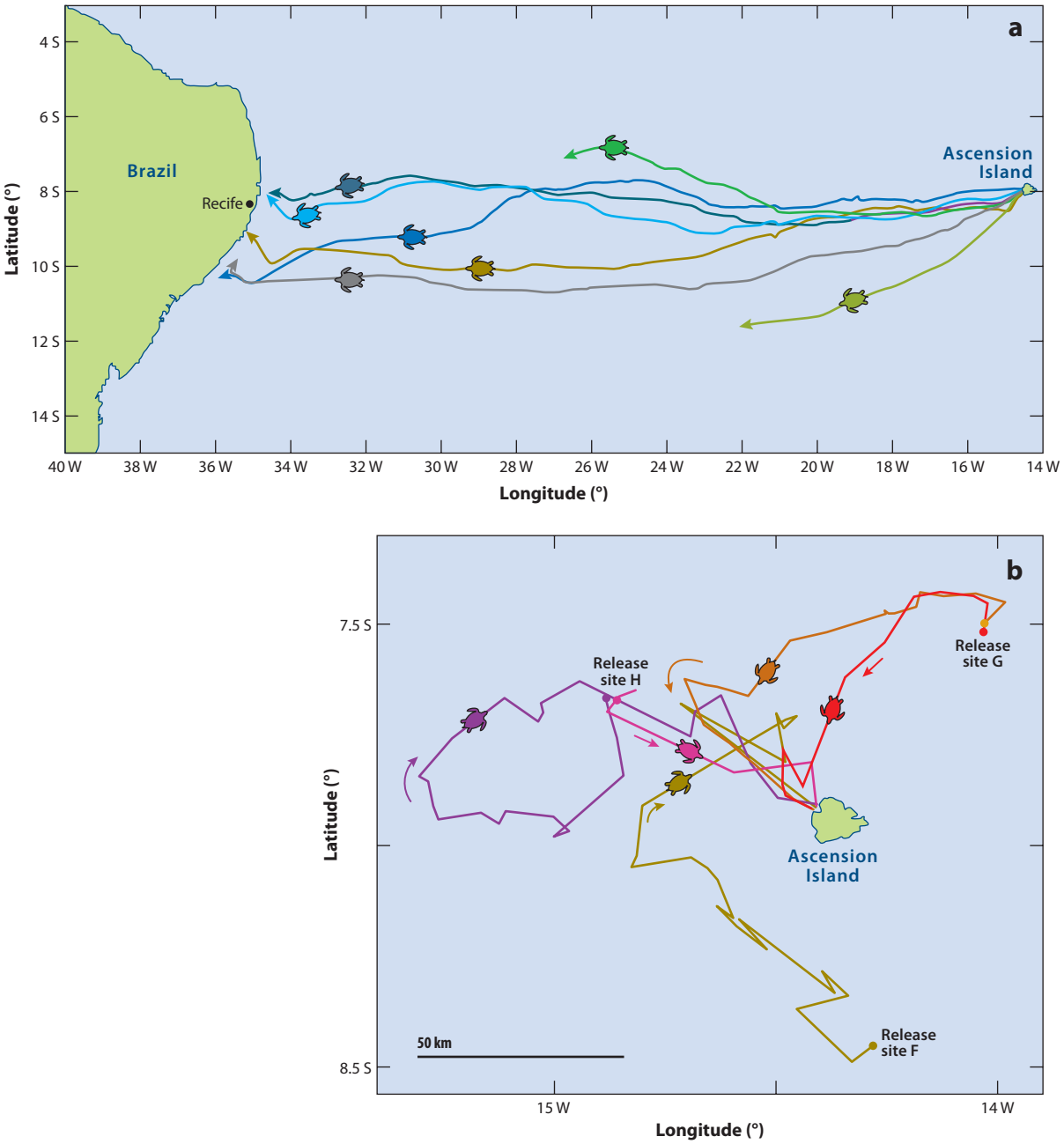

Figure 9

Turtle tracks. (*a*) Westward migration of magnetically disturbed turtles. Panel *a* redrawn from Papi et al. (2000). (*b*) The return to Ascension Island of five turtles displaced to sites south, northwest, and northeast for F, G, and H, respectively. Panel *b* redrawn from Luschi et al. (2001).

of visual clues must be ruled out, including the use of star maps); (*c*) compensation for current drift; and (*d*) compensation for forced displacements that can be large in magnitude, both in distance and orientation. The ability to find a dot in the middle of nowhere is not unique to sea turtles. As Papi & Luschi (1996) and Akesson (1996) have noted, there are interesting similarities in some of the seemingly routine navigational feats of albatrosses, which travel thousands of kilometers simply to find food, returning easily to their original home/nesting sites, which are often very small islands. It is possible that a series of position fixes could occur in the outbound navigation of both sea turtles and albatrosses and that these can be memorized and used on the return journey.

It is also possible that the notion of an apparently featureless ocean or atmosphere is not correct and that there are reliable clues embedded in the swirling winds and currents, much as demonstrated for the stratified wakes of bluff bodies (Section 2) and of islands (Section 3). Over mesoscales, the vortical wake motions are affected by the background density gradient, and the coherence in these layers can propagate to form more regular patterns even in the mixed surface layers. This was demonstrated on a very large scale over thousands of kilometers for the Hawaiian Island chain for which the coherent wake induced large-scale disturbances that then propagated owing to planetary rotation effects, making observable and dynamically significant changes in the sea-surface temperature. A second point is that although the conceptual model for island wakes is often one inspired by time-averaged turbulence models, in which an average plume spreads out over an average distance, the instantaneous velocity and scalar fields (which are what are sensed) vary quite considerably in geometry and amplitude (e.g., of concentration and velocity gradients) from the mean. The pattern and geometry of the wakes in **Figures 1** and **2** do not resemble slowly diffusing plumes.

We may examine the case of the green sea turtle in more detail. The outbound migration, from Ascension Island to Brazil, occurs roughly as shown in **Figure 9*a***, for both magnetically disturbed and undisturbed individuals. The tracks appear to slowly fan out and then at some point keep going due west or even converge. Equation 8 gives a purportedly universal prediction for the spreading of an initial turbulent wake under the influence of stratification. Although the undersea topography of an island is more appropriately described as a conical column rather than a finite three-dimensional bluff body, the layering of neighboring patches is likely to produce local regions whose evolution roughly follows these empirical laws. In fact, one may even expect this kind of evolution in the unstratified, surface mixed layers because the scaling in terms of $\mathrm{Fr}_{\mathrm{mom}}$ and Nt is such that stratification parameters are unimportant, so the wake width is

$$\frac{L_y}{D} = C_0(x/D)^{C_1}, \tag{14}$$

where constants $C_{0,1}$ do not differ significantly from their unstratified counterparts up to $x/D = 10^4$. For a 10-km diameter island, this gives an ideally traceable wake length (in a perfectly quiet ocean) of greater length than any ocean basin. If the wake does persist, even in a noisy background, then at $x = 2{,}200$ km, $L_y/D \approx 0.28(x/D)^{0.35}$ and $L_y \approx 18$ km. In **Figure 9*a***, the maximum spread of the tracks of the westward-bound turtles is ≈400 km, already many times the nominal wake width. Approximately 700 km into the journey, however, the majority of the tracks are much more compact, with about a 60-km spread. The laboratory experiment in a quiet tank is likely to be much more compact and orderly than the ocean wake, although the Jan Mayen example in **Figure 6** is not that dissimilar. It does seem reasonable, however, that the turtles are swimming and navigating inside the island wake in the first part of their journey.

In original tracking experiments on westward-bound turtles, Luschi et al. (1998) noted that the initial part of the tracks (looking much like those shown in **Figure 9*a***) was very closely aligned with the South Atlantic Equatorial Current. Buoy measurements and numerical models show that

the South Atlantic Equatorial Current is very steady and predictable in the months of May–July, with a west-southwest direction (255–260°). The turtles were reported to spend roughly 90% of the time submerged, diving for periods between 4 and 16 min, and it was suggested that these dives might be related to the turtles exploring the depth profile of a chemical/odor plume from the island. Later in their journey, it appears the turtles apply a correction that takes them across the likely prevailing currents. If the current direction information is correct, then the turtles may be switching to an alternative mechanism to navigate the remainder of the trip. The final approach once again aligns with the predicted current direction.

The most mysterious part of the migration is in the return trip, in the ability to home in on the small dot. In the catch-and-release displacement experiments of Luschi et al. (2001), the successful return path was conspicuously not from the west-southwest direction, but from the northwest (**Figure 9**). At the same time, a reconstruction of geomagnetic field parameters showed no systematic clues that were being exploited by the searching turtles, who could not find the island from the southeast (Akesson et al. 2003). The prevailing winds are the trade winds from the southeast, and their direction appears to be strongly correlated with the final approach, as noted above. The last leg into the prevailing wind (and not water) currents could be following a chemical tracer, modified surface wave patterns, or perhaps a wake defect, this time airborne.

It is quite unlikely that the migratory feats of the green sea turtle can be explained by any one navigational mechanism, but it is plausible that the compact, long-lived island wakes, in both air and water, are usable. Finally, time-depth recorders attached to turtles migrating to Ascension Island have shown a most-interesting diving pattern that includes shallow dives down to 10 m or so, and much longer and deeper dives, to 30 m and more (Hays et al. 2001). The authors suggested that these dives may be ways to avoid presenting obvious silhouettes to predators, although their true function is hard to discern. The return tracks to Ascension Island were on displaced turtles, always within 270 km of the nesting sites. In both outbound and inbound turtles that are so close to the island, there could be useful submerged information that significantly helps their navigational accuracy. The prevalence of concentrated and orderly wake information makes such apparently energetically costly behavior understandable as a water-sampling strategy. The purpose of the deeper dives would be to access the most-concentrated source of water currents and chemical tracers in the stratified waters at the head of the thermocline. They could be sampled in a profiling dive or while an animal is momentarily at rest on the bottom.

4. PREDATOR DETECTION OF HYDRODYNAMIC TRAILS

Another class of wakes and wake detectors may be found in predator-prey relations, most recently investigated in some detail in aquatic animals. In these studies, the longevity and persistence of the prey-induced wake signature are often noted with some surprise, as is the ability of the hunter to find and follow the information upstream to its creator. We are far from the classical regime in which stratification is likely to have an effect on the vortex wake geometry. Instead, a more general cause of the pattern persistence could be in the relatively organized wake flows that a swimmer makes in the first place.

4.1. Fish Wakes

Lighthill (1969) first suggested that the carangiform mode of locomotion of fast swimming fish, in which large-amplitude oscillations are primarily confined to a tail with moderate to high aspect ratio, would produce in its three-dimensional form a chain of approximately circular vortex rings.

He noted that the circular ring conveys maximum momentum per unit kinetic energy and that the meager data available at the time supported the selection of kinematics and geometry to make this plausible. The widespread adoption of particle image velocimetry (PIV) measurement techniques has provided evidence that a wake model of a string of interconnected, almost circular, ring shapes is quite reasonable (Lauder & Drucker 2002; Müller et al. 1997; Nauen & Lauder 2002a,b; Stamhuis & Videler 1995; Videler 1993; Videler & He 2010; Videler et al. 2002). Increasingly detailed measurements (e.g., Hu et al. 2005) and computations (Zhu et al. 2002) show many variations and small-scale, intricate patterns that do not readily conform to one standard topology, but the basic idea seems sound.

Fish wakes can be quite long lived and compact. Hanke et al. (2000) measured late wakes of goldfish and found that they could easily be detected for up to 3 min after passage of the fish. For a fish with a 10-cm body length, L, then $x/L \approx 20$ or $x/D \approx 100$ for a fineness ratio of 5 fish. A comparison with vortex ring kinematics (Weigand & Gharib 1997) showed a narrower wake than that observed for laminar vortex rings carefully created by a piston, and further persistent fish wakes have been measured by Hanke & Bleckmann (2004).

The fish wake contains predictable length and velocity scale information. Anderson et al. (1998) showed that propulsive efficiencies approaching 90% could be achieved by oscillating hydrofoils and that the optimal kinematics were closely linked with the production of optimal wake patterns. For moderate thrust coefficients, high efficiency was obtained when $St_{wake} = 0.3–0.4$, where St_{wake} is defined as usual but where the length scale is the total wake width, or twice the oscillation amplitude. The range is consistent with the later and broader compilation by Taylor et al. (2003), showing that most swimming and flying animals indeed operate with $St_{wake} \in \{0.2–0.4\}$. Dabiri (2009) demonstrated that the range of St_{wake} can be described as a preferred range of vortex formation numbers, in which the shed vorticity is efficiently accumulated into the coherent wake structures. Without further detail, it is clear that (*a*) animal wakes can have stable and long-lived structures and that (*b*) there is predictable length and timescale information in them.

4.2. Seals

Harbor seals live in water that is not always transparent and must have some direction-finding capability when optical clues are weak or absent, such as in darkness, great depths, or just in murky water conditions. Lacking the well-known sonar of dolphins, for example, alternative sensing systems were thought to be present. Moreover, that blind and apparently healthy seals have been found in the wild further suggests some kind of mechanism for navigation around the environment and for prey capture. Dehnhardt et al. (1998) performed the first study showing that the long facial whiskers (or vibrissae) of harbor seals can detect very small water currents and their variation. A harbor seal was trained to indicate detectable currents induced by a submerged, vertically oscillating sphere. The frequency and amplitude of vibrations were correlated with characteristics of the hydrodynamic disturbance, and the seal was shown to be able to detect flow speeds of less than 0.5 mm/s at frequencies from 25 to 50 Hz. No detection was possible when the whiskers were covered with a wire mesh mask, when currents could impinge on the whiskers but they could not interact with the flow. The detection thresholds were orders of magnitude below expected stimulus magnitudes from fish wakes (see the previous section).

An even more striking study followed (Dehnhardt et al. 2001) that demonstrated that the harbor seal could track the hydrodynamic wakes of a small submerged, propeller-driven submarine (**Figure 10**). The submarine was driven on a straight or curved course and then powered down. The wake detection trial began when headphones were removed from the test subject. When the submarine path was not straight, the seal would track the wake exactly and would not take

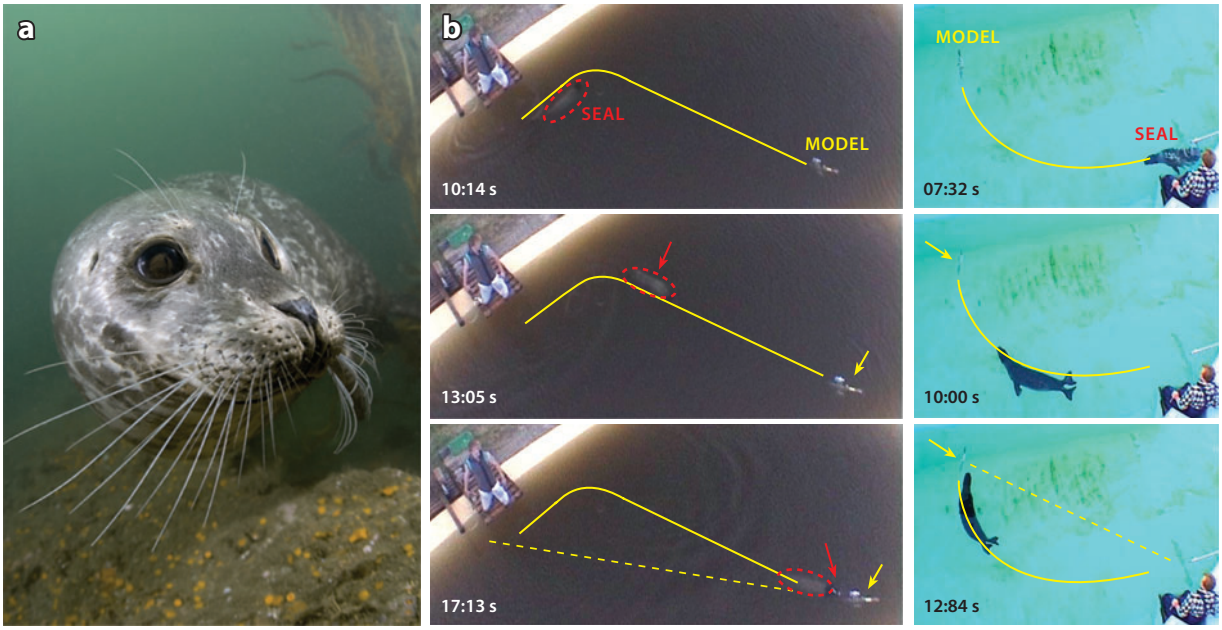

Figure 10

A harbor seal and its tracks. (*a*) Harbor seal in Monterey Bay. The larger whiskers appear to have two alternating lengths. Photograph taken by Kawika Chetron and reproduced by kind permission of his family. (*b*) Tracking of curved minisubmarine wakes by a blindfolded, and initially acoustically masked, harbor seal. The seal position is shown by the red arrow and the model by the yellow arrow. When the submarine motor is turned off, the seal follows the curved track (*solid yellow*). When the motor is left on, idling, the seal makes a direct line to its location (*dashed lines*). Panel *b* taken from Dehnhardt et al. (2001), reprinted with permission from AAAS.

a straight-line shortcut to the current position of the idle submarine. In one set of trials, the submarine passed either left-right or right-left approximately 1 m in front of the seal. In 46 out of 50 trials, the correct direction was immediately chosen. If the submarine motor was left on, then the seal would make a straight-line path to the acoustic source.

The submarine wake was reported to have a characteristic width $W_{\text{sub}} \leq 60$ cm after 20 s. A self-propelled wake in the limit of low stratification (high Fr) is narrower than its unpropelled counterpart, by an amount that depends not only on the over- or underthrust [no submarine would reach equilibrium, steady-state motion in the strict sense of Meunier & Spedding (2006) in these experiments], but also on propeller geometry, but very roughly has a characteristic width approximately one-half of the equivalent towed body. At $t = 60$ s, we find that $Ut = x = 40$ m, and x/D would be 800 for a 5-cm-diameter model. From Spedding (1997), we expect $L_y/D \approx 2$ for the nonpropelled wake, and so $L_y/D \approx 1$ here. If the submarine has $D = 5$ cm, then the wake width should also be of similar magnitude. That reported widths are many times this value could be a result of background currents, the nonsteady motion (small accelerations and turning) of the submarine, or different ways of defining a width. The protracted whiskers had a span $W_{\text{vib}} \approx 25$ cm, and side-to-side tracking movements would approximately double this search width. It is quite likely that W_{vib} suffices to cover a large fraction of the target wake width and/or a number of coherent structures therein.

Further studies on biologically generated wakes, with their more compact and organized structure (Schulte-Pelkum et al. 2007) and on wakes of varying ages (Wieskotten et al. 2010a), confirmed the results of the initial studies. If there are adaptations to increase sensitivity to certain expected

EDDY RHEOCHEMOTAXIS

This article concentrates on fluid mechanical wakes and their detection, concerning chemical tracers and other scalars only incidentally. This kind of distinction is not maintained by some biological wake-detecting systems. A case in point is the smooth dogfish, studied by Gardiner & Atema (2007). Sharks have a well-developed sense of smell and can find prey by following odor trails alone. In an intriguing experiment, sharks were placed at the downstream end of an 8-m flume. Laminar trails of food-rich material and just plain seawater were produced upstream. These trails were then obliged to turn over a submerged brick and mix in its turbulent wake. Experiments were performed in different lighting conditions and with intact sharks or those with their lateral line system disabled. The lateral line is responsible for detecting water currents, both mean and fluctuating in time and with spatial variation. Intact sharks preferred the odor trails with turbulence. Those with their lateral line lesioned did not or could not distinguish between the different hydrodynamic signatures, and when the lights were turned off, they could not distinguish between food-rich and plain seawater trails. The best search efficiency depended on a combination of smell, hydrodynamics, and visual clues. Atema (1996) introduced the term eddy rheochemotaxis to describe orientation by both odor and current in flavored eddies, for lobsters tracking plumes. This work continues with both real and robotic lobsters (Grasso et al. 1998, 2000).

types of wake geometry, then the tracking success could be sensitive to deliberate modifications of it, and Wieskotten et al. (2012b) showed that a remotely piloted submarine in burst-and-glide motion significantly disrupts the tracking success in open-pool wake-following experiments. This is not unexpected because when in almost-steady motion, the main wake will be overthrusted (to overcome all drag components, including wave drag and the drag of control surfaces), and in glide mode, it will revert to a drag wake, with the direction of the central wake reversed. Intermittent or burst-and-glide swimming is common in naturally behaving fish, and although it is usually seen as a means of minimizing energy expenditure (Weihs 1974), the authors noted that the resulting wakes could also be systematically more difficult to detect than those coming from steady swimming.

The impressive ability of harbor seals to detect hydrodynamic wake signatures has motivated efforts to design, test, and build biomimetic versions (e.g., Eberhardt et al. 2011, Hanke et al. 2000, Valdivia y Alvarado et al. 2012, Witte et al. 2012), and in some cases, aspects of their unusual undulating geometry are also being tested (Hans et al. 2012) with promising results. The rush to test biomimetic whisker-based wake detectors is not always accompanied by thorough control experiments (what other detectors could work?), but the topic promises to be vibrant and engaging for some time to come.

Hydrodynamic and chemical information traces are frequently combined in wakes from the natural environment (be they islands or fish; see the sidebar Eddy Rheochemotaxis), and the following section gives an example where this combination is important owing to the much smaller scale.

4.3. Copepods

Copepods are small crustaceans with typical body lengths of 1–2 mm (**Figure 11*a***). They are found in almost all forms of freshwater (from puddles to lakes) and in the sea form a major component of plankton, occupying a critical part of the food chain between microbial algae and phytoplankton and larger juvenile and adult fish, seabirds, and sea mammals. Copepods can occur in dense swarms and arguably compose the largest biomass on Earth. Their long antennae and other appendages have arrays of microsetae that are quite sensitive to small variations, and patterns of variation, in impinging water currents. They are light sensitive but have no image-forming eyes.

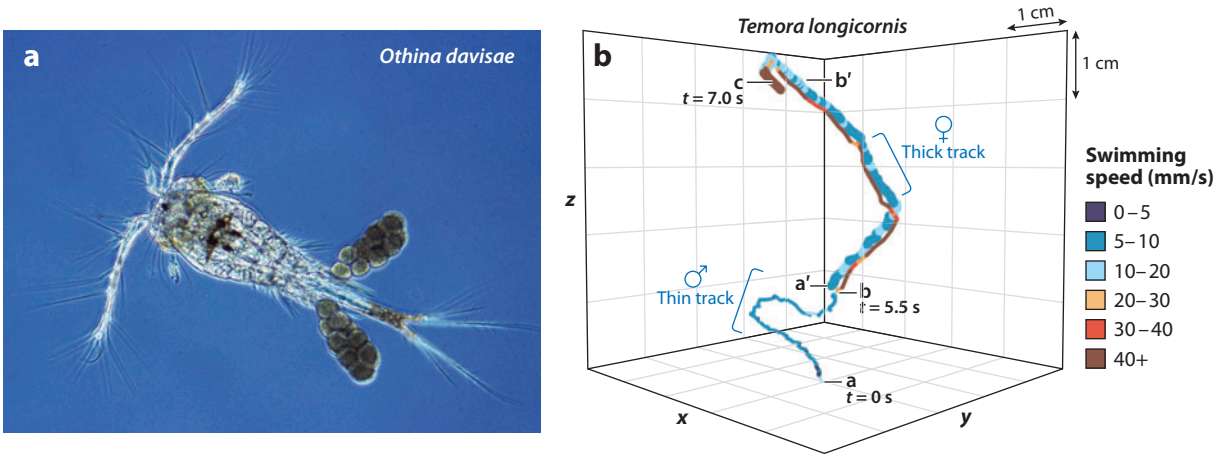

Figure 11

A copepod and its tracks. (*a*) The marine copepod *Othina davisae*. Multiple bristles can be seen at multiple scales. Photograph by Albert Calbet, reproduced with permission. (*b*) The tracking of a female *Temora longicornis* (*thick track*) by a male (*thin track*). At times when the male is positions a, b, and c, the female is at a′, b′, and c. Panel *b* adapted from Doall et al. (1998) by permission of the Royal Society.

It is often remarked that most animals' principal concerns can be summarized into three categories: (*a*) acquiring food, (*b*) avoiding being food, and (*c*) finding a mate. The last problem is quite serious for small animals with apparently limited and primarily proximal sensory information. The ability of copepods to sense and respond to water currents and chemical signals is critical to their survival.

4.3.1. Copepod wake generation and tracking. Quite remarkable discoveries have been made concerning the chemical and hydrodynamic disturbances that copepods can create and sense. Yen (2000) gave an overview of a world in which different sized copepods, moving at different speeds, find themselves in an intricate balance between viscous-dominated small scales, smaller than a Kolmogorov scale, and momentary pulses of inertial motion of the animal and/or its wake. The characteristic Reynolds numbers range from 10^{-2} to 10^{3}, when substantially different locomotion strategies will be appropriate. In keeping with their three critical life imperatives, copepods have three principal swimming strategies: (*a*) hovering while generating feeding current, (*b*) cruising, and (*c*) moving into a fast escape response (or mate capture).

A mix of chemical and hydrodynamic wakes is left behind each individual copepod, the balance between them depending on the Reynolds number. Molecular diffusivities of small pheromone-type chemicals are expected to be approximately 10^{-5} cm^2/s, and the kinematic viscosity of seawater is approximately 10^{-2} cm^2/s, so the Schmidt number Sc $\approx 10^{3}$. Chemical trails can be laid down and will persist for much longer times than hydrodynamic wake disturbances. Nevertheless, the latter do seem to be important. Van Duren et al. (1998) showed that in the presence of males, females greatly increase the frequency of characteristic hopping motions, which leave about a 12-fold increase in the hydrodynamic wake signature length, thus increasing their chances of being detected by interested males. The hops are thought to be energetically expensive and so are probably not undertaken lightly.

A thorough description of chemical and hydrodynamic wake generation (by females) and tracking (by males) by the copepod *Temora longicornis* has been reported by Doall et al. (1998), Weissburg

et al. (1998), and Yen et al. (1998). Males could detect female wakes aged up to 10 s over distances of 130*L*. Upon encountering a trail, the male abruptly changes course and tracks it very closely (**Figure 11*b***). A tracking male doubles his speed while following the chemical trail, a behavior that not only allows him to catch up, but also thins the viscous boundary layer over chemical receptors. When within 1–2*L*, the male accelerates rapidly and latches onto the female. It also disrupts the very wake that he is tracking, making it much more difficult for any follower or copier to stay in touch. This is the region that is characterized most strongly by the hydrodynamic wake. The near wake will be a mix of chemical and hydrodynamic patterns, and Yen (2000) spoke of the "eddy packaging" of odors, a concept quite analogous to the flavor eddies of island wakes.

Tracking of long chemical trails for *Centropages typicus* has been described by Bagoien & Kiorboe (2005), who showed males successfully following complex tracks and occasionally being disrupted by intervening small-scale flow irregularities that come either from irregular female swimming or from the environment. *C. typicus* has $L \approx 1.5$ mm and can successfully track trails of 17 cm in length, again $>100L$.

A quite complex picture emerges of the hydrochemical and social dynamics of the copepod. When in swarms, the characteristic spacing between animals can be much less than either the hydrodynamic wake length or the chemical trail length, so the mix of animals, hydrodynamic signatures, flavored eddies, and chemical trails is a complex that allows reliable communication in the low-Re life at Kolmogorov scales. Encounters between mates and signaling with neighbors are much better than mere chance, with wake pattern information providing the link.

5. SUMMARY/CONCLUSIONS

5.1. General Principles?

It appears to be normal that wakes comprising arrays of coherent structures have long lifetimes, whether the locally compact organization comes from a cyclical generation mechanism (fish tail) or from constraints on an otherwise fully turbulent wake (stratified wakes). The pattern is maintained for long times and large distances, but individually measurable quantities evolve with time and distance, so a spot measurement of a characteristic speed or length scale cannot uniquely be traced to a specific upstream condition. Two measurements separated in time might help, but the coordinate origin is still not determined. Therefore, other information is needed. For the navigating sea turtle, this could be an internal clock that measures how long it has been in the migration. For a submerged, self-propelled body (e.g., fish, submarine) detector, it could be a spatial range of possible origins and a finite list of candidate sizes. In any event, the comparatively recently developed appreciation for both the ubiquity and the persistence of patterns and structures over a very broad range of scales, from millimeters to thousands of kilometers, opens new possibilities for understanding natural phenomena (e.g., plankton swarms, turtle navigation, ocean transport in mesoscale eddies) and for improved and increasingly sophisticated mapping, exploration, and detection.

5.2. Information and Pattern

Common coherent structure patterns in a number of wakes are associated with stability, long life, and then the possibility of detection. Because the natural environment is full of patterns, detection is inextricably a signal/noise problem but one that should be imagined on the instantaneous fields, not on real or imagined time and space averages. The LCS identification efforts are well suited for this idea, and the FTLE ridges between structures represent the Lagrangian traces of real material transport. These structures have been shown to be tracked by frigate birds presumably following concentrations of food-rich water (Kaia et al. 2009). It is less clear how an often-convoluted FTLE

track could be used by a navigator wishing to make a direct approach to an object embedded in the flow. The problem of navigation in an instantaneous scalar field, and the notion of such fields as intermittent information sources, has been addressed by Vergassola et al. (2007), who proposed an infotaxis search algorithm for odor-detecting moths and plume-tracking robots alike. Reasonable search algorithms for intermittent, noisy, and multicomponent data have been considered also by Hein & McKinley (2012), who noted that the absence of signal is not the same as the absence of information and that mixed search strategies that adapt to recent inputs can be successful and match well with observations.

Both the recurring phenomenon of wake persistence and the extraordinary ability of navigating animals are noted above. We have much to learn about pattern identification and extraction, particularly using and fusing multiple sensors and sensor modalities. When the multiple data sources are combined with geometric ideas that characterize relevant fluid dynamics, perhaps along the lines of Perry & Chong (1987) and Chong et al. (1990) or along the more recent LCS trajectory (Farazmand & Haller 2012, Haller 2011, Haller & Beron-Vera 2012), a hint of the information capacity of the ocean and atmospheric currents, and their possible deciphering and exploitation, may be revealed.

SUMMARY POINTS

1. The fluid environment is replete with complex, but structured motions, over a very large range of scales.
2. There are numerous mechanisms for making especially robust signals in this environment, and many observers are surprised by the longevity of wake structures, from islands, submarines, fish, and zooplankton.
3. The endurance of the wake leads to newly recognized possibilities for information transmission and detection.

FUTURE ISSUES

1. We may anticipate developments in the synthesis of information (just as animals do). Now that new modes of data acquisition are available, with unprecedented scope (resolution in time and space), the focus may shift to analysis and information extraction and characterization.
2. Recognizing the patterned environment, we may focus also on disruption of the natural state: This can be deliberate (for camouflage) or an incidental product of pollution/accidents.
3. Biomimetic systems are partly interesting as models of information acquisition and assimilation in ways that are foreign to us, owing to differences in either scale and/or sensor design and modality. Synthetic, augmented biomimetic systems could form part of a new assimilation and characterization program.

DISCLOSURE STATEMENT

The author is not aware of any biases that might be perceived as affecting the objectivity of this review.

ACKNOWLEDGMENTS

The core research on turbulence in stratified fluids has had continued support from the Office of Naval Research, most recently under grant N00014-11-1-0553 administered by Dr. R. Joslin. This support is most gratefully acknowledged. I especially thank Susanne Åkesson of Lund University and Jeannette Yen of Georgia Tech for inspiring and lively conversations and Trystan Madison and Xinjiang Xiang at USC for research assistance.

LITERATURE CITED

Afanasyev YD. 2004. Wakes behind towed and self-propelled bodies: asymptotic theory. *Phys. Fluids* 16:3235–38

Akesson S. 1996. News and comment: geomagnetic map used for long-distance navigation? *Trends Ecol. Evol.* 11:398–400

Akesson S, Broderick A, Glen F, Godley BJ, Luschi P, et al. 2003. Navigation by green turtles: Which strategy do displaced adults use to find Ascension Island? *Oikos* 103:363–72

Describes a range of migratory feats, with many navigational and locomotion efficiency implications.

Alerstam T, Hedenström A, Åkesson S. 2003. Long-distance migration: evolution and determinants. *Oikos* 103:247–60

Amini N, Hassan YA. 2012. An investigation of matched index of refraction technique and its application in optical measurements of fluid flow. *Exp. Fluids* 53:2011–30

Anderson JM, Streitlien K, Barrett DS, Triantafyllou MS. 1998. Oscillating foils of high propulsive efficiency. *J. Fluid Mech.* 360:41–72

Atema J. 1996. Eddy chemotaxis and odor landscapes: exploration of nature with animal sensors. *Biol. Bull.* 191:129–38

Augier P, Billant P. 2011. Onset of secondary instabilities on the zigzag instability in stratified fluids. *J. Fluid Mech.* 682:120–31

Augier P, Chomaz JM, Billant P. 2012a. Spectral analysis of the transition to turbulence from a dipole in stratified fluid. *J. Fluid Mech.* 713:86–108

Augier P, Galtier S, Billant P. 2012b. Kolmogorov laws for stratified turbulence. *J. Fluid Mech.* 709:659–70

Bagoien E, Kiorboe T. 2005. Blind dating: mate finding in planktonic copepods. I. Tracking the pheromone trail of *Centropages typicus*. *Mar. Ecol. Prog. Ser.* 300:105–15

Barale V, Gower JFR, Alberotanza L, eds. 2010. *Oceanography from Space: Revisited*. New York: Springer

Barton ED. 2009. Island wakes. In *Ocean Currents: A Derivative of the Encyclopedia of Ocean Sciences*, ed. JH Steel, SA Thorpe, KK Turekian, pp. 470–75. New York: Academic

Barton ED, Flament P, Dodds H, Mitchelson-Jacob EG. 2001. Mesoscale structure viewed by SAR and AVHRR near the Canary Islands. *Sci. Mar.* 65:167–75

Beron-Vera FJ, Olascoaga MJ, Brown MG, Kocak H. 2010. Invariant-tori-like Lagrangian coherent structures in geophysical flows. *Chaos* 20:017514

Beron-Vera FJ, Olascoaga MJ, Goni GJ. 2008. Oceanic mesoscale eddies as revealed by Lagrangian coherent structures. *Geophys. Res. Lett.* 35:L12603

Bevilaqua PM, Lykoudis PS. 1978. Turbulence memory in self-preserving wakes. *J. Fluid Mech.* 89:589–606

Applies a new scaling argument for strongly stratified flows, where the flow selects the vertical scale.

Billant P, Chomaz JM. 2001. Self-similarity of strongly stratified inviscid flows. *Phys. Fluids* 13:1645–51

Bonneton P, Chomaz JM, Hopfinger EJ. 1993. Internal waves produced by the turbulent wake of a sphere moving horizontally in a stratified fluid. *J. Fluid Mech.* 254:23–40

Bonnier M, Bonneton P, Eiff O. 1998. Far-wake of a sphere in a stably stratified fluid: characterization of vortex structures. *Appl. Sci. Res.* 59:269–81

Bonnier M, Eiff O. 2002. Experimental investigation of the collapse of a turbulent wake in a stratified fluid. *Phys. Fluids* 14:791–801

Bonnier M, Eiff O, Bonneton P. 2000. On the density structure of far-wake vortices in a stratified fluid. *Dyn. Atmos. Oceans* 31:117–37

Brethouwer G, Billant P, Lindborg E, Chomaz JM. 2007. Scaling analysis and simulation of strongly stratified turbulent flows. *J. Fluid Mech.* 585:343–68

Chomaz JM, Bonetton P, Hopfinger EJ. 1993. The structure of the near wake of a sphere moving horizontally in a stratified fluid. *J. Fluid Mech.* 254:1–21

Chong MS, Perry AE, Cantwell BJ. 1990. A general classification of three-dimensional flow fields. *Phys. Fluids A* 2:765–77

Dabiri JO. 2009. Optimal vortex formation as a unifying principle in biological propulsion. *Annu. Rev. Fluid Mech.* 41:17–33

Dehnhardt G, Mauck B, Bleckmann H. 1998. Seal whiskers detect water movements. *Nature* 394:235–36

Dehnhardt G, Mauck B, Hanke W, Bleckmann H. 2001. Hydrodynamic trail-following in harbor seals (*Phoca vitulina*). *Science* 293:102–4

Deloncle A, Billant P, Chomaz JM. 2008. Nonlinear evolution of the zigzag instability in stratified fluids: a shortcut on the route to dissipation. *J. Fluid Mech.* 599:229–39

Diamessis PJ, Domaradzki JA, Hesthaven JS. 2005. A spectral multidomain penalty method model for the simulation of high Reynolds number localized incompressible stratified turbulence. *J. Comput. Phys.* 202:298–322

Diamessis PJ, Spedding GR, Domaradzki JA. 2011. Similarity scaling and vorticity structure in high Reynolds number stably stratified turbulent wakes. *J. Fluid Mech.* 671:52–95

Doall MH, Colin SP, Strickler JR, Yen J. 1998. Locating a mate in 3D: the case of *Temora longicornis*. *Philos. Trans. R. Soc. Lond. B* 353:681–89

Dommermuth DG, Rottman JW, Innis GE, Novikov EA. 2002. Numerical simulation of the wake of a towed sphere in a weakly stratified fluid. *J. Fluid Mech.* 473:83–101

Dong C, McWilliams JC. 2007. A numerical study of island wakes in the Southern California Bight. *Cont. Shelf Res.* 27:1233–48

Dong C, McWilliams JC, Shchepetkin AF. 2007. Island wakes in deep water. *J. Phys. Oceanogr.* 37:962–81

Eberhardt W, Shakhsheer Y, Calhoun B, Paulus J, Appleby M. 2011. A bio-inspired artificial whisker for fluid motion sensing with increased sensitivity and reliability. In *IEEE Sensors 2011*, pp. 982–85. New York: IEEE

Farazmand M, Haller G. 2012. Computing Lagrangian coherent structures from their variational theory. *Chaos* 22:013128

Gardiner JM, Atema J. 2007. Sharks need the lateral line to locate odor sources: rheotaxis and eddy chemotaxis. *J. Exp. Biol.* 210:1925–34

Godoy-Diana R, Chomaz JM, Billant P. 2004. Vertical length scale selection for pancake vortices in strongly stratified viscous fluids. *J. Fluid Mech.* 504:229–38

Gourlay MJ, Arendt SC, Fritts DC, Werne J. 2001. Numerical modeling of initially turbulent wakes with net momentum. *Phys. Fluids* 13:3783–802

Grasso FW, Basil JA, Atema J. 1998. Toward the convergence: robot and lobster perspectives of tracking odors to their source in the turbulent marine environment. In *Proc. Intelligent Control* (*ISIC*), pp. 259–64. New York: IEEE

Grasso FW, Consi TR, Mountain DC, Atema J. 2000. Biomimetic robot lobster performs chemo-orientation in turbulence using a pair of spatially separated sensors: progress and challenges. *Robot. Auton. Syst.* 30:115–31

Hafner J, Xie SP. 2003. Far-field simulation of the Hawaiian wake: sea surface temperature and orographic effects. *J. Atmos. Sci.* 60:3021–32

Haller G. 2001. Distinguished material surfaces and coherent structures in 3D fluid flows. *Physica D* 149:248–77

Haller G. 2002. Lagrangian coherent structures from approximate velocity data. *Phys. Fluids* 14:1851–61

Haller G. 2011. A variational theory of hyperbolic Lagrangian coherent structures. *Physica D* 240:574–98

Haller G, Beron-Vera FJ. 2012. Geodesic theory of transport barriers in two-dimensional flows. *Physica D* 241:1680–702

Hanke W, Bleckmann H. 2004. The hydrodynamic trails of *Lepomis gibbosus* (Centrarchidae), *Colomesus psittacus* (Tetraodontidae) and *Thysochromis ansorgii* (Cichlidae) investigated with scanning particle image velocimetry. *J. Exp. Biol.* 207:1585–96

Hanke W, Brücker C, Blackmann H. 2000. The ageing of the low-frequency water disturbances caused by swimming goldfish and its possible relevance to prey detection. *J. Exp. Biol.* 203:1193–200

Presents a comprehensive classification of fluid flow topology based on the analysis of reduced equations.

Provides the first high–Reynolds number direct numerical simulation of stratified and unstratified turbulent wakes.

Along with Haller (2002, 2011), presents the first development of theory of LCS and solution trajectories in dynamical systems/fluid models.

Hans H, Miao J, Triantafyllou M. 2012. Characterization of von Kármán street with seal whisker-like sensor. In *IEEE Sensors 2012*. New York: IEEE. doi: 10.1109/ICSENS.2012.6411583

Hays GC, Åkesson S, Broderick A, Glen F, Godley BJ, et al. 2001. The diving behaviour of green turtles undertaking oceanic migration to and from Ascension Island: dive durations, dive profiles and depth distribution. *J. Exp. Biol.* 204:4093–98

Hein AM, McKinley SA. 2012. Sensing and decision-making in random search. *Proc. Natl. Acad. Sci. USA* 109:12070–74

Higuchi H, Kubota T. 1990. Axisymmetric wakes behind a slender body including zero-momentum configurations. *Phys. Fluids* 2:1615–23

Provides a modern treatise on turbulence, 70 years on from Kolmogorov.

Holmes P, Lumley JL, Berkooz G, Rowley CW, eds. 2012. *Turbulence, Coherent Structures, Dynamical Systems and Symmetry*. Cambridge, UK: Cambridge Univ. Press. 2nd ed.

Hu DL, Mendel L, Chan B, Goreau T, Bush JW. 2005. Visualization of a fish wake using tobacco mosaic virus. *Phys. Fluids* 17:091103

Johansson PBV, George WK, Gourlay MJ. 2003. Equilibrium similarity, effects of initial conditions and local Reynolds number on the axisymmetric wake. *Phys. Fluids* 15:603–17

Kaia ET, Rossi V, Sudre J, Weimerskirch H, Lopez C, et al. 2009. Top marine predators track Lagrangian coherent structures. *Proc. Natl. Acad. Sci. USA* 106:8245–50

Lauder GV, Drucker EG. 2002. Forces, fishes, and fluids: hydrodynamic mechanisms of aquatic locomotion. *Physiology* 17:235–40

Lekien F, Coulliette C, Mariano AJ, Ryan EH, Shay LK, et al. 2005. Pollution release tied to invariant manifolds: a case study for the coast of Florida. *Physica D* 210:1–20

Presents an epic and original synthesis of fluid mechanics and biology over a large range of Reynolds numbers.

Lighthill MJ. 1969. Hydromechanics of aquatic animal propulsion. *Annu. Rev. Fluid Mech.* 1:413–46

Lilly DK. 1983. Stratified turbulence and the mesoscale variability of the atmosphere. *J. Atmos. Sci.* 40:749–61

Lin JT, Pao YH. 1974. *Turbulent wake of a self-propelled slender body in stratified and non-stratified fluids: analysis and flow visualizations*. APL/JHU POR-3586, Flow Res. Rep. 11, Appl. Phys. Lab., Seattle

Lin JT, Pao YH. 1979. Wakes in stratified fluids. *Annu. Rev. Fluid Mech.* 11:317–38

Lin Q, Lindberg WR, Boyer DL, Fernando HJS. 1992. Stratified flow past a sphere. *J. Fluid Mech.* 240:315–54

Lindborg E. 2006. The energy cascade in a strongly stratified fluid. *J. Fluid Mech.* 550:207–42

Lohmann KJ. 2010. Nature Q&A: magnetic-field perception. *Nature* 464:1140–42

Lohmann KJ, Lohmann CMF, Ehrhart LM, Bagley DA, Swing T. 2004. Geomagnetic map used in sea-turtle navigation. *Nature* 428:909–10

Luschi P, Åkesson S, Broderick A, Glen F, Godley BJ, et al. 2001. Testing the navigational abilities of ocean migrants: displacement experiments on green sea turtles (*Chelonia mydas*). *Behav. Ecol. Sociobiol.* 50:528–34

Luschi P, Hays GC, del Seppia C, Marsh R, Papi F. 1998. The navigational feats of green sea turtles migrating from Ascension Island investigated by satellite telemetry. *Proc. R. Soc. Lond. B* 265:2279–84

Meunier P, Spedding GR. 2004. A loss of memory in stratified momentum wakes. *Phys. Fluids* 16:298–303

Meunier P, Spedding GR. 2006. Stratified propelled wakes. *J. Fluid Mech.* 552:229–56

Müller UK, van den Heuvel BLE, Stamhuis EJ, Videler JJ. 1997. Fish foot prints: morphology and energetics of the wake behind a continuously swimming mullet (*Chelon labrosus* Risso). *J. Exp. Biol.* 200:2893–906

Nauen JC, Lauder GV. 2002a. Hydrodynamics of caudal fin locomotion by chub mackerel, *Scomber japonicus* (Scombridae). *J. Exp. Biol.* 205:1709–24

Nauen JC, Lauder GV. 2002b. Quantification of the wake of rainbow trout *Oncorynchus mykiss* using three-dimensional stereoscopic digital particle image velocimetry. *J. Exp. Biol.* 205:3271–79

Pao HP, Kao TW. 1976. On vortex trails over ocean islands. *Atmos. Sci. J. Meterol. Soc. Rep. China* 3:28–38

Papi F, Luschi P. 1996. Pinpointing 'Isla Meta': the case of sea turtles and albatrosses. *J. Exp. Biol.* 199:65–71

Papi F, Luschi P, Åkesson S, Capogrossi S, Hays GC. 2000. Open-sea migration of magnetically disturbed sea turtles. *J. Exp. Biol.* 203:3435–43

Provides an important early work on topological descriptions of fluid flows through critical points.

Perry AE, Chong MS. 1987. A description of eddying motions and flow patterns using critical-point concepts. *Annu. Rev. Fluid Mech.* 19:125–55

Putnam NF, Endres CS, Lohmann CMF, Lohmann KJ. 2011. Longitude perception and bicoordinate magnetic maps in sea turtles. *Curr. Biol.* 21:463–66

Reed AM, Milgram JH. 2002. Ship wakes and their radar images. *Annu. Rev. Fluid Mech.* 34:469–502

Riley JJ, de Bruyn Kops SM. 2003. Dynamics of turbulence strongly influenced by buoyancy. *Phys. Fluids* 15:2047–59

Riley JJ, Lelong MP. 2000. Fluid motion in the presence of strong stratification. *Annu. Rev. Fluid Mech.* 32:613–57

Riley JJ, Metcalf RW, Weissman MA. 1981. Direct numerical simulations of turbulence in homogeneously stratified fluids. In *Nonlinear Properties of Internal Waves*, ed. BJ West, pp. 79–112. New York: Am. Inst. Phys.

Robinson IS. 2004. *Measuring Oceans from Space: The Principles and Methods of Satellite Oceanography*. New York: Springer

Robinson IS. 2010. *Discovering the Ocean from Space: The Unique Applications of Satellite Oceanography*. New York: Springer

Sasaki H, Xie SP, Taguchi B, Nonaka M, Masumoto Y. 2010. Seasonal variations of the Hawaiian lee countercurrent induced by the meridional migration of the trade winds. *Ocean Dyn.* 60:705–15

Schetz JA, Jakubowski AK. 1975. Experimental study of the turbulent wake behind self-propelled slender bodies. *AIAA J.* 13:1568–75

Schooley AH, Stewart RW. 1962. Experiments with a self-propelled body submerged in a fluid with vertical density gradient. *J. Fluid Mech.* 15:83–99

Schulte-Pelkum N, Wieskotten S, Hanke W, Dehnhardt G, Mauck B. 2007. Tracking of biogenic hydrodynamic trails in harbour seals (*Phoca vitulina*). *J. Exp. Biol.* 210:781–87

Settles GS. 2006. Fluid mechanics and homeland security. *Annu. Rev. Fluid Mech.* 38:87–110

Shadden SC, Lekien F, Marsden JE. 2005. Definition and properties of Lagrangian coherent structures from finite-time Lyapunov exponents in two-dimensional aperiodic flows. *Physica D* 212:271–304

Shadden SC, Lekien F, Paduan JD, Chavez FP, Marsden JE. 2009. The correlation between surface drifters and coherent structures based on high-frequency radar data in Monterey Bay. *Deep-Sea Res. II* 56:161–72

Spedding GR. 1997. The evolution of initially turbulent bluff-body wakes at high internal Froude number. *J. Fluid Mech.* 337:283–301

Spedding GR, Browand FK, Fincham AM. 1996a. The long-time evolution of the initially turbulent wake of a sphere in a stable stratification. *Dyn. Atmos. Ocean* 23:171–82

Spedding GR, Browand FK, Fincham AM 1996b. Turbulence, similarity scaling and vortex geometry in the wake of a towed sphere in a stably stratified fluid. *J. Fluid Mech.* 314:53–103

Stamhuis EJ, Videler JJ. 1995. Quantitative flow analysis around aquatic animals using laser sheet particle image velocimetry. *J. Exp. Biol.* 198:283–94

Taylor GK, Nudds RI, Thomas ALR. 2003. Flying and swimming animals cruise at a Strouhal number tuned for high power efficiency. *Nature* 425:707–11

Tennekes H, Lumley JL. 1972. *A First Course in Turbulence*. Cambridge, MA: MIT Press

Townsend AA. 1976. *The Structure of Turbulent Shear Flow*. Cambridge, UK: Cambridge Univ. Press. 2nd ed.

Valdivia y Alvarado P, Subramaniam V, Triantafyllou M. 2012. Design of a bio-inspired whisker sensor for underwater applications. In *IEEE Sensors 2012*. New York: IEEE. doi: 10.1109/ICSENS.2012.6411517

van Duren LA, Stamhuis EJ, Videler JJ. 1998. Reading the copepod personal ads: increasing encounter probability with hydromechanical signals. *Philos. Trans. R. Soc. Lond. B* 353:691–700

Veneziani M, Griffa A, Garraffo ZD, Chassignet EP. 2005. Lagrangian spin parameter and coherent structures from trajectories released in a high-resolution ocean model. *J. Mar. Res.* 63:753–88

Vergassola M, Villermaux E, Shraiman BI. 2007. 'Infotaxis' as a strategy for searching without gradients. *Nature* 445:406–9

Videler JJ. 1993. *Fish Swimming*. London: Chapman & Hall

Videler JJ, He P. 2010. Swimming in marine fish. In *Behavior of Marine Fishes: Capture Processes and Conservation Challenges*, ed. P He, pp. 3–24. New York: Wiley-Blackwell

Videler JJ, Stamhuis EJ, Müller UK, van Duren LA. 2002. The scaling and structure of aquatic animal wakes. *Integr. Comput. Biol.* 42:988–96

Voropayev SI, Afanasyev YD. 1994. *Vortex Structures in a Stratified Fluid*. London: Chapman & Hall

Waite ML, Bartello P. 2003. Stratified turbulence dominated by vortical motion. *J. Fluid Mech.* 517:281–308

Weigand A, Gharib M. 1997. On the evolution of laminar vortex rings. *Exp. Fluids* 22:447–57

Presents an influential review of strongly stratified flows and is a starting point for the current one.

Rigorously applies LCS theory to practical examples.

Weihs D. 1974. Energetic advantages of burst-and-coast swimming of fish at high speeds. *J. Theor. Biol.* 48:215–29

Weissburg MJ, Doall MH, Yen J. 1998. Following the invisible trail: kinematic analysis of mate-tracking in the copepod *Temora longicornis*. *Philos. Trans. R. Soc. Lond. B* 353:710–12

Wieskotten S, Dehnhardt G, Mauck B, Miersch L, Hanke W. 2010a. Hydrodynamic determination of the moving direction of an artificial fin by a harbour seal (*Phoca vitulina*). *J. Exp. Biol.* 213:2194–200

Wieskotten S, Dehnhardt G, Mauck B, Miersch L, Hanke W. 2010b. The impact of glide phases on the trackability of hydrodynamic trails in harbour seals (*Phoca vitulina*). *J. Exp. Biol.* 213:3734–40

Witte M, Hanke W, Wieskotten S, Miersch L, Brede M, et al. 2012. On the wake flow dynamics behind Harbor Seal vibrissae: a fluid mechanical explanation for an extraordinary capability. *Notes Numer. Fluid Mech. Multidiscip. Des.* 119:271–89

Wolanski E, Imberger J, Heron ML. 1984. Island wakes in shallow coastal waters. *J. Geophys. Res.* 89:10553–69

Woods AW. 2010. Turbulent plumes in nature. *Annu. Rev. Fluid Mech.* 42:391–412

Xie SP, Liu WT, Liu Q, Nonaka M. 2001. Far-reaching effects of the Hawaiian islands on the Pacific ocean-atmosphere system. *Science* 292:2057–60

Yang Y, Ma J, Xie SP. 2008a. Observations of the trade wind wakes of Kauai and Oahu. *Geophys. Res. Lett.* 35:L04807

Yang Y, Xie SP, Hafner J. 2008b. The thermal wake of Kauai Island: satellite observations and numerical simulations. *J. Clim.* 21:4568–86

Yen J. 2000. Life in transition: balancing inertial and viscous forces by planktonic copepods. *Biol. Bull.* 198:213–24

Yen J, Weissburg MJ, Doall MH. 1998. The fluid physics of signal perception by mate-tracking copepods. *Philos. Trans. R. Soc. Lond. B* 353:787–804

Young GS, Zawislak J. 2006. An observational study of vortex spacing in island wake vortex streets. *Mon. Weather Rev.* 134:2285–94

Zhu Q, Wolfgang MJ, Yue DKP, Triantafyllou MS. 2002. Three-dimensional flow structures and vorticity control in fish-like swimming. *J. Fluid Mech.* 468:1–28

Provides a novel and thorough analysis of oceanographic and satellite data to show the surprising influence of the Hawaiian Islands across the Pacific Ocean.